# CHAPTER IV

# RESULTS AND DISCUSSIONS

## 4.1 Design and synthesis of curcumin derivatives

**Curcumin** was investigated as a potential anti-cancer agent by inducing apoptosis [42]. Furthermore, the **curcumin** also was used as a fluorescence dye because of a delocalization of electron via $\pi$-conjugated double bond and aromatic rings systems. Hence, we also employed **curcumin** as both anti-cancer and fluorescence imaging agents.

Chaicham et al. [58] have reported the synthesis of the novel curcumin derivatives including, **$CurBF_2$**, **$CurBF_2OTs$** and **$CurBF_2(OTs)_2$**. The synthesis pathway was illustrated in Scheme 4.1. Difluoroboron curcumin derivative, **$CurBF_2$**, was obtained by the replacement of borontrifluoride diethytherate to enolate unit of **Curcumin**. Mono and di-tosylated (**$CurBF_2OTs$** and **$CurBF_2(OTs)_2$**) were synthesized by the reaction between **$CurBF_2$** and tosyl chloride. The coordination of $BF_2$ could encourage the planarity structure of **curcumin**, which led to the improvement of the optical property of **curcumin**. In addition, the **curcumin** scaffold of **$CurBF_2$**, **$CurBF_2OTs$** and **$CurBF_2(OTs)_2$** was also expected to function as anti-cancer agent. All of samples were characterized by $^1$H-NMR spectroscopy.

Actaully, **curcumin** shows a poor solubility in aqueous solution, which was the limitation of bioavailability and clinical efficiency. In this research, we have focused on the synthesis of curcumin derivatives and improvement of the stabilities of curcumin derivatives by using self-assembled coordination nanoparticles for further biological tasks.

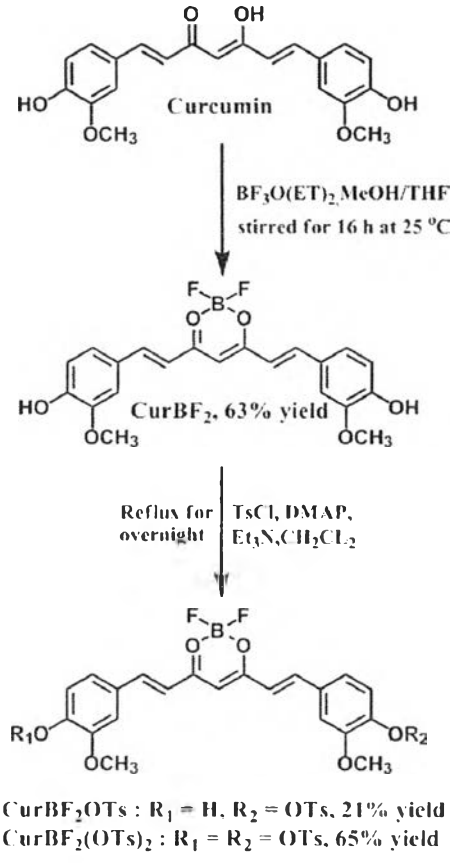


**Scheme 4.1** Synthetic pathway of curcumin derivatives

### 4.1.1 Synthesis and characterization of curcumin borondifluoride ($CurBF_2$)

The desired **$CurBF_2$** was prepared by **curcumin** illustrated in Scheme 4.1. The solution of **curcumin** was added by the borontrifluoride diethyl etherate, providing a change of bright yellow to red solution. The residual was purified by precipitation using methanol and ethyl acetate to obtain the red solid of desired compound in 63 % yield. The borondifluoride moiety, which is electron withdrawing group, was interacted on the $\beta$-diketone moiety based **curcumin** to yield **$CurBF_2$**. The $^1$H-NMR spectrum of **$CurBF_2$** showed the downfield shift of all proton signals due to electron withdrawing of **$BF_2$** group as shown in Figure 4.1. The methoxy protons of **$CurBF_2$** appeared 1 peaks at 3.83 ppm indicating the same environment of $OCH_3$ on the end of benzene rings.

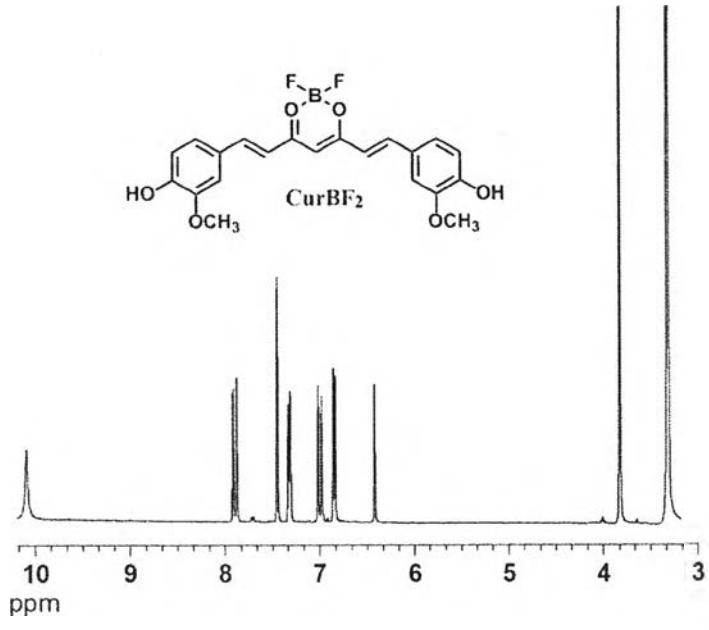


**Figure 4.1** The $^{1}$H-NMR spectrum of **CurBF$_2$** in DMSO-d$_6$

### 4.1.2 Synthesis and characterization of curcumin borondifluoride mono-tosylation (CurBF$_2$OTs) and di-tosylation borondifluoride (CurBF$_2$(OTs)$_2$)

**CurBF$_2$OTs** and **CurBF$_2$(OTs)$_2$** were obtained from the nucleophilic substitution reaction of **CurBF$_2$** and *p*-toluenesulfonyl chloride and using triethylamine as base in dichloromethane at 0 °C under nitrogen atmosphere. The mixture compounds were purified by column chromatography using 5% ethyl acetate in dichloromethane to give **CurBF$_2$OTs** and **CurBF$_2$(OTs)$_2$** in 21 % and 65 % yield, respectively. The $^{1}$H-NMR spectrum of **CurBF$_2$OTs** (Figure 4.2) displayed the characteristic peaks of tosylate protons at 2.42 ppm corresponding to 3 protons of Ar-C*H*$_3$, as well as 7.25 and 7.7 ppm assigned to the additional aromatic protons of tosyl group. The $^{1}$H-NMR spectrum of **CurBF$_2$(OTs)$_2$** (Figure 4.3) displayed the different patterns from **CurBF$_2$OTs**. The methoxy protons of monoTs appeared 2 peaks at 3.90 and 3.56 ppm indicating the different environment of OC*H*$_3$ on the end of benzene rings.

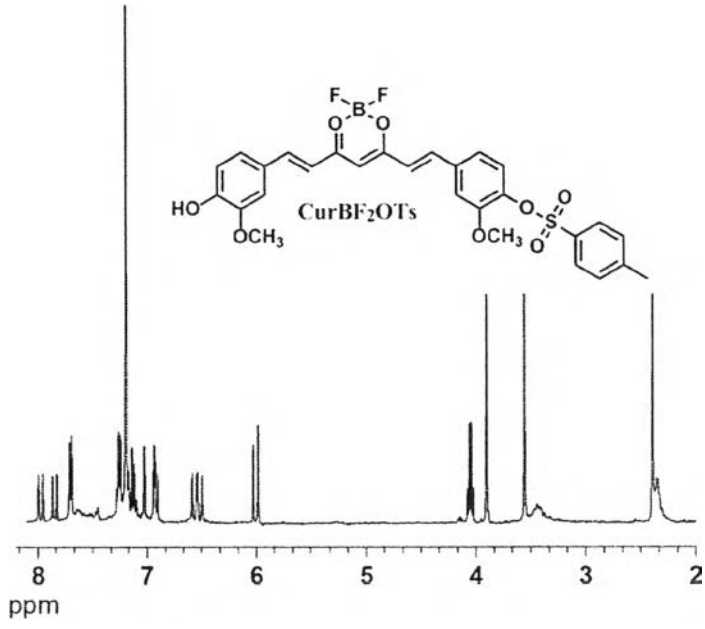


**Figure 4.2** $^{1}$H -NMR spectrum of **CurBF$_2$OTs** in $CDCl_3$

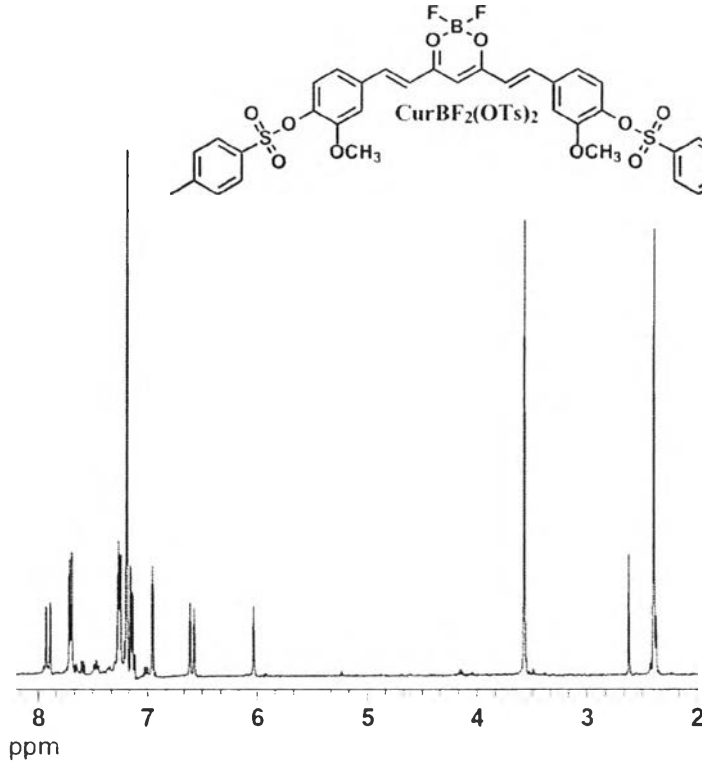


**Figure 4.3** $^{1}$H -NMR spectrum of **CurBF$_2$(OTs)$_2$** in $CDCl_3$

## 4.2 Self-assembly of coordination nanoparticles (CNPs)

Nanoparticles were applied in many disciplines, particularly in medical or biological systems as drug delivery into the target cells. Self-assembly of supramolecular structures was prepared by using transition metal ions and synthetic ligands, which have been used to enhance the encapsulation ability of molecules and nanoscale materials in supramolecular networks. The ability of encapsulated molecule of nanomaterials could improve their functions for technologically important applications [10-14].

We have focused on the preparation of the novel coordination nanoparticles from gadolinium ions ($Gd^{3+}$) and surfactants for stabilizing the curcumin derivatives in buffers solution. In this research, we have investigated the influence of the type of surfactants and buffers on the size and morphology of coordination nanoparticles. The samples were prepared by different surfactants including SDS (anionic), CTAB (cationic) and Triton X-100 (neutral) and various buffers including HEPES, MOPS, Tris and phosphate. Their structures were shown in Figure 4.4.

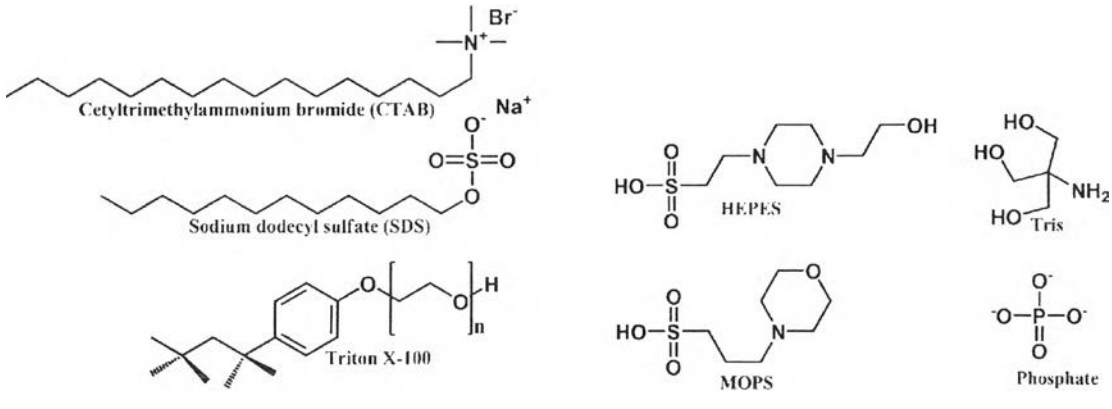


**Figure 4.4** Chemical structures of surfactants and buffers

### 4.2.1 Size and structural morphology characterizations

The denominations and various conditions of the samples discussed were collected in the Table 4.1.

**Table 4.1** Identification, composition of the samples prepared at room temperature

| Sample name | Lanthanide | Surfactant | Buffer | Dye or Drug |
|---|---|---|---|---|
| **GdCH** | $Gd^{3+}$ | CTAB | HEPES | None |
| **GdTxH** | $Gd^{3+}$ | Triton X-100 | HEPES | None |
| **GdSH** | $Gd^{3+}$ | SDS | HEPES | None |
| **GdSM** | $Gd^{3+}$ | SDS | MOPS | None |
| **GdST** | $Gd^{3+}$ | SDS | Tris | None |
| **GdSP** | $Gd^{3+}$ | SDS | phosphate | None |
| **GdSH-Cur** | $Gd^{3+}$ | SDS | HEPES | **curcumin** |

The TEM images of the **GdCH**, **GdTxH**, **GdSH**, **GdSM** and **GdST CNPs** and SEM image of **GdSP CNPs** were shown in Figures 4.5 and 4.6. The **GdSH CNPs** in Figure 4.5(c) showed mostly spherical particle shape. The particles formed a large, compact, and network structure, implying agglomeration small-sized primary particles from the innitial formation. These phenomena agree with the formation of transition metal oxide particle at ambient conditions reported by Holzinger and Kickelbick [67].

Dynamic light scattering (DLS) was employed to determine the particles size of coordination nanoparticles in aqueous solution. The particle sizes of samples were summarized in Table 4.2, which showed average size from counting particles as determined from TEM images and DLS technique.

The average sizes from counting 200 particles in TEM images showed that the particle size of **GdSH CNPs** are slightly larger than **GdTxH** and **GdCH** particles, which were prepared by SDS anionic, Triton X-100 non-ionic and CTAB cationic surfactants, respectively (as shown in Figure 4.5).

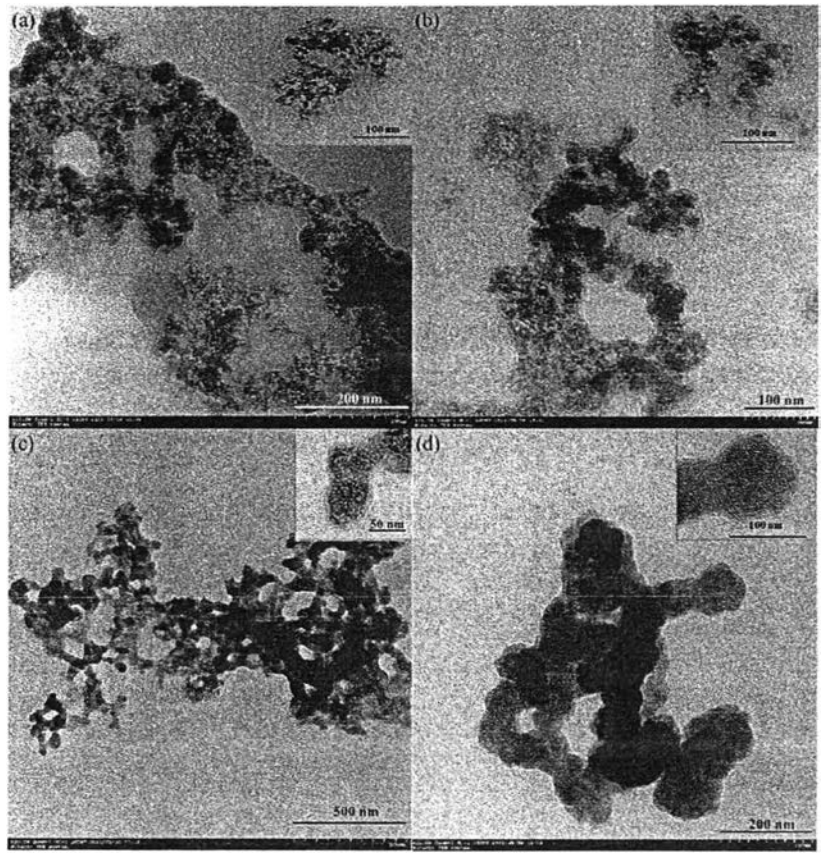


**Figure 4.5** TEM images of **GdCH** (a), **GdTxH** (b), **GdSH** (c) and **GdSH-Cur** (d)

**Table 4.2** Average sizes of the samples prepared at room temperature were determined by TEM and DLS technique

| Sample name | Average size by TEM(nm) | Average size by DLS(nm) |
|---|---|---|
| **GdCH** | 21 ± 17 | 92.08 |
| **GdTxH** | 20 ± 15 | 115.65 |
| **GdSH** | 65 ± 13 | 140.65 |
| **GdSM** | 62 ± 16 | 160.83 |
| **GdST** | 50 ± 8 | 222.60 |
| **GdSP** | Not observed | 598.10 |
| **GdSH-Cur** | 71 ± 15 | 157.67 |

Moreover, the particle sizes of **GdSH CNPs** measured by DLS method were larger than those of **GdTxH** and **GdCH CNPs**. Possibly, the particle sizes of nanoparticles might be dependent on the ionic properties of surfactants. The gadolinium ions might prefer to form with anionic surfactant over cationic and non-

ionic surfactants. Another reason for the dependence of the particle size is the different amphiphilic characteristic of three surfactant. Therefore, the particle size of **CNPs** from SDS is larger than that of **CNPs** from Triton X-100 and CTAB.

The overall particle size of coordination nanoparticles determined by TEM was generally rather smaller than that of coordination nanoparticles measured by DLS. Since, the TEM image was investigated in the dried air condition, but the DLS data was measured in the water. As a consequent, the hydration layer from water was addressed and showed a larger hydrodynamic diameter [68].

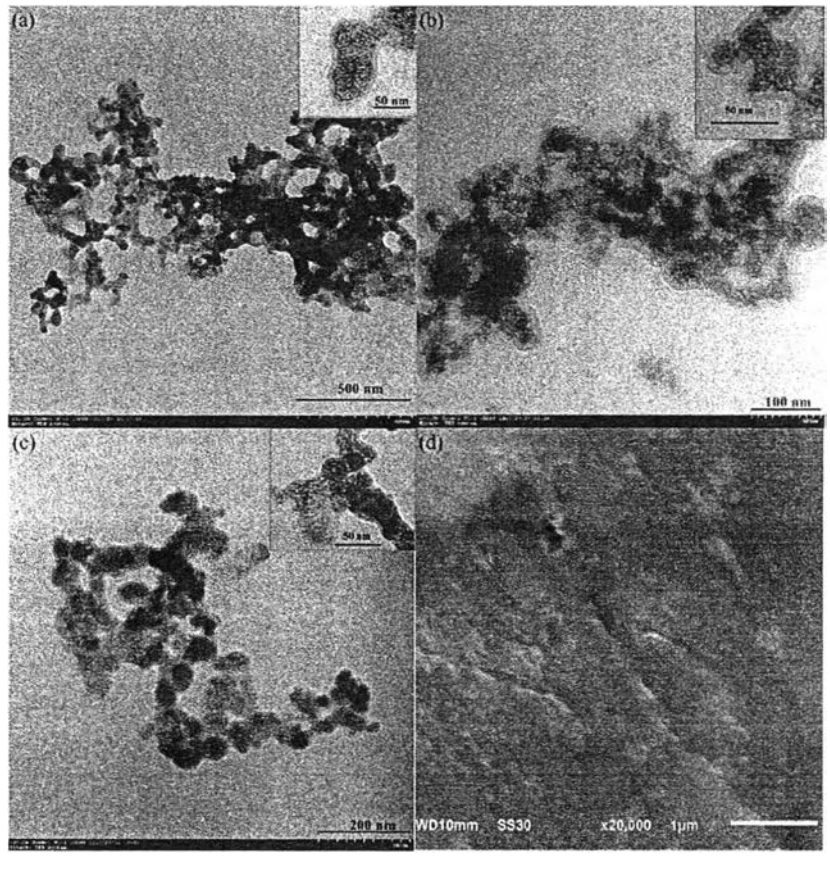


**Figure 4.6** TEM images of **GdSH** (a), **GdSM** (b), **GdST** (c) and SEM image of **GdSP** (d)

Buffers should be considerably realized in the formation of coordination nanoparticles. Thereby, HEPES, MOPS, Tris and phosphate buffers were examined. According to the TEM and SEM images in Figure 4.6, the coordination nanoparticles prepared in HEPES buffer (**GdSH CNPs**) showed slightly larger size than those prepared in MOPS (**GdSM CNPs**) and Tris (**GdST CNPs**), while the coordination nanoparticles in phosphate buffer (**GdSP CNPs**) were observed. From the Figure A2

(in Appendix), the particles size distribution of **GdSH** is unity compared to those of **GdSM**, **GdST** and **GdSP**.

However, it is still unclear about the formation mechanism of coordination nanoparticles by $Gd^{3+}$, surfactant and buffer. Nonetheless, the well-known method for the preparation of nano-drug delivery in the colloidal form is the microemulsion method. The microemulsion particle size ~ 10-200 nm was prepared by surfactant and the co-surfactant in two solvent phases in order to produce the flexibility between oil/water interfaces. The co-surfactant would insert between each of the surfactant molecule and subsequently form the nano-size of particles [18] as shown in Figure 4.7.

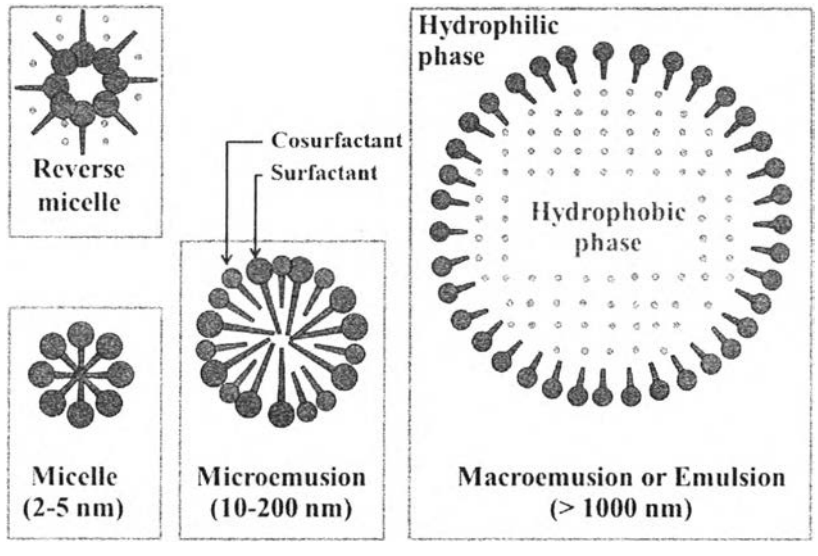


**Figure 4.7** Structures of Micelle, Microemulsion, Emulsion and Reverse micelle [18]

From the DLS information, the particle size of **GdSH** from HEPES buffer was obviously smaller than those of **GdSM** from MOPS, **GdST** from Tris and **GdSP** from phosphate, respectively. Assuming that the buffer inserted between SDS by hydrophobicity and also employed the sulfate anion based HEPES to form electrostatic interactions with $Gd^{3+}$. Interestingly, we hypothesized that the hydroxyl group could form hydrophilicity with water inducing the reverse-microemulsion structure dissolved in water.

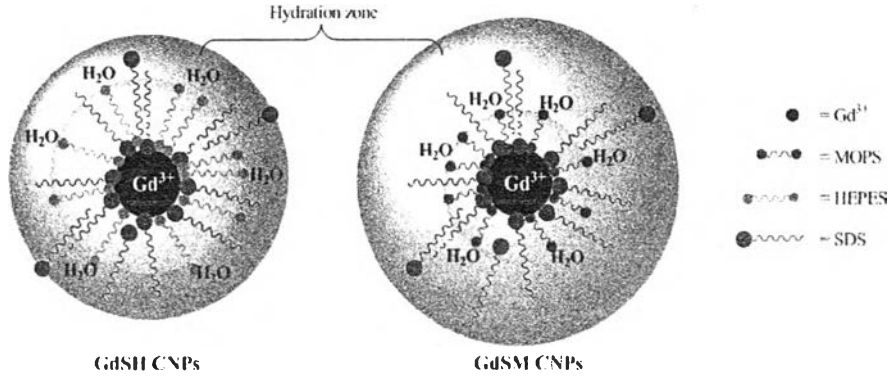


**Scheme 4.2** Postulated structure of **GdSH CNPs** and **GdSM CNPs**

Considering the particle sizes by DLS, MOPS and Tris buffers showed a larger particle size of **CNPs** than HEPES buffer. This can be explained that MOPS and Tris contain a shorter chain hydroxy group. The outer sphere of hydration layer of water is closed to the $Gd^{3+}$ core inducing the swelling particles and a large distribution of particle size. Compared to **GdSH**, HEPES acts as a co-surfactant which has a long chain. The outer sphere of hydration layer of water is far from $Gd^{3+}$ ion allowing a high compact of surfactant and co-surfactant and a consequently small particles size in DLS analysis (as shown in Scheme 4.2).

In the case of phosphate buffer, the particle size was very large and over the range of microemulsion size. It implied that the phosphate buffer might form the emulsion structure instead of the microemulsion form.

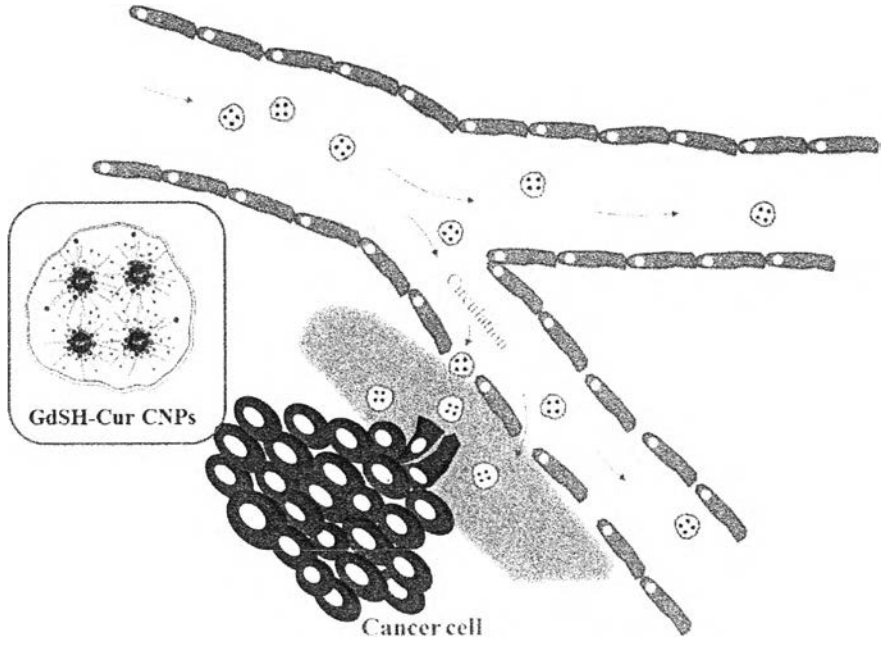


**Scheme 4.3** Schematic illustration of **GdSH-Cur CNPs** delivered to cancer cell via EPR effect

In addition, the TEM image of **curcumin** doped in coordination nanoparticles (**GdSH-Cur CNPs**) was showed in Figure 4.5(d). The DLS data showed an increase of particle size of **GdSH-Cur CNPs** after an encapsulation of **curcumin** in coordination nanoparticles from 140.65 nm to 157.57 nm. As successful approach, a crucial aspect of drug delivery development involves the particle size of the coordination nanoparticles, which enable to pass through the leaky tumor blood vessels of the target tumor cell by a conceptual illustration in Scheme 4.3 [15-17].

### 4.2.2 Infrared spectroscopy

FT-IR spectroscopy was used to study the formation of the coordination nanoparticles. FT-IR spectra (Figure 4.8) showed the vibrational spectra of the pure surfactants and the respective prepared samples. The C–H transmission bands appeared between 2800 and 3000 $cm^{-1}$ in all of the pure surfactant spectra. Considerably, the appearance of C-H transmission band was observed in the case of **GdSH CNPs**. Moreover, the band of the sulfate group of SDS was slightly shifted to lower wavenumbers from 1219, 1081 and 994 to 1189, 1067 and 974 $cm^{-1}$, respectively. This evidence strongly suggested the occurrence of the coordinated formation between sulfate of SDS and $Gd^{3+}$ [23].

Additionally, the disappearance of the characteristic peak of $NO_3^-$ at 1634 $cm^{-1}$ in all FT-IR spectra of samples confirmed that the sulfate group based SDS could interact on the surface of $Gd^{3+}$ ions instead of the nitrate group. In comparison of CTAB and Triton x-100, SDS showed strong interactions with $Gd^{3+}$ ion.

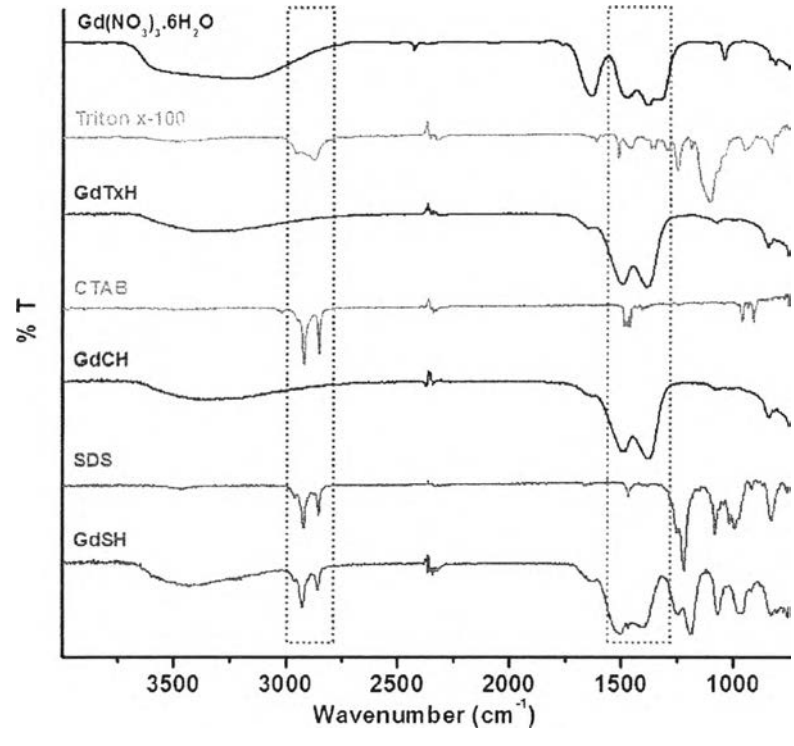


**Figure 4.8** FT-IR spectra of the three pure surfactants and **CNPs** from the respective surfactants

According to the FT-IR spectra in Figure 4.9, the observation of the board peak at 1310-1590 $cm^{-1}$ was due to C-O stretching vibration of carbonate, which was actually formed by the mechanism of the oxidic lanthanide materials and carbon dioxide under ambient conditions [69]. This peak has not been observed in the case of **GdSP** sample. The SDS characteristic peak in the range of 2800-3000 $cm^{-1}$ did not appear in the FTIR-spectrum of **GdSP** sample. However, the spectrum displayed the phosphate characteristic peak from 880-1140 $cm^{-1}$. These suggested that the phosphate buffer could not be contracted with the $Gd^{3+}$ and SDS to form the nanoparticles. The SDS characteristic peaks from 2800-3000 $cm^{-1}$ appeared in FT-IR spectra even in the case of HEPES, MOPS and Tris. This suggested that HEPES, MOPS and Tris are an assistance for formation of coordination nanoparticles.

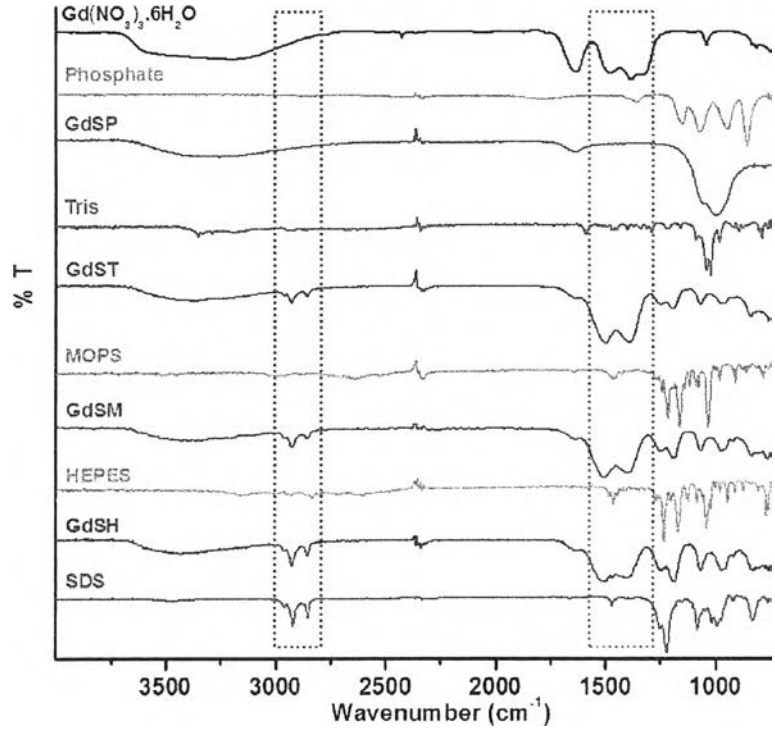


**Figure 4.9** FT-IR spectra of the pure SDS, pure $Gd(NO_3)_3.6H_2O$, four pure buffer and **CNPs** from the respective buffer

**Table 4.3** SDS assignment mode, in the absence and and in the presence of Gd nanoparticles

| Peak assignment [24] | Peak position ($cm^{-1}$) | |
|---|---|---|
| | SDS | **GdSH CNPs** |
| $\nu_{asym}$ (C-H) | 2917 | 2921 |
| $\nu_{sym}$ (C-H) | 2850 | 2854 |
| $\delta_s$ (C-H) | 1468 | - |
| $\nu_{asym}$ (-$SO_3$-) | 1219 | 1189 |
| $\nu_{sym}$ (-$SO_3$-) | 1081 | 1067 |

$\nu$ = stretching, sym = symmetric, asym = antisymmetric, $\delta_s$ = methylene scissoring.

The stabilized formation mechanism of coordination nanoparticles under the surfactant coated on the surface of Gd nanoparticles via terminal functional groups was observed by FT-IR spectrum of pure SDS and SDS-coated Gd nanoparticle (**GdSH**) in Figure 4.9. The characteristic main peaks were assigned in Table 4.3. The results showed peak shift from the originated functional group of SDS, which indicated the binding of relatively close-packed surfactant monolayer on the nanoparticles surface [70]. To investigate the interaction of sulfate on $Gd^{3+}$ nanoparticles surface, the wave number separation ($\Delta$) of $\nu_{asym}$ (-$SO_3$-) and that ($\Delta$) of $\nu_{sym}$ (-$SO_3$-) based on SDS before and after coordinating with $Gd^{3+}$ was demonstrated. Previous results showed the different binding modes of -$SO_3$- and metal nanoparticles, such as monodentate, bidentate or bidentate bridging and ionic interactions. The wave number separations ($\Delta$) in the range of <110 $cm^{-1}$, 200-320 $cm^{-1}$and 140-190 $cm^{-1}$ were reported corresponding to monodentate, bidentate bridging and chelating bidentate, respectively. [71]. For this research, $\Delta$ of $\nu_{asym}$ (-$SO_3$-) was 30 $cm^{-1}$ (1219-1189 $cm^{-1}$) and $\Delta$ of $\nu_{sym}$ (-$SO_3$-) was 14 $cm^{-1}$ (1081-1067 $cm^{-1}$). The data illustrated that sulfate group of SDS molecule covalently bonded to the $Gd^{3+}$ nanoparticles surface via monodentate bound mode. Moreover, the **GdSH CNPs** displayed the protective layer of steric SDS molecule via both electrostatic repulsion and steric hindrance [24]. As anticipated, we proposed that the HEPES buffer would be included

in the surface of **GdSH CNPs**. The possible mechanism of synthesis of the coordination nanoparticles was illustrated in Scheme 4.4.

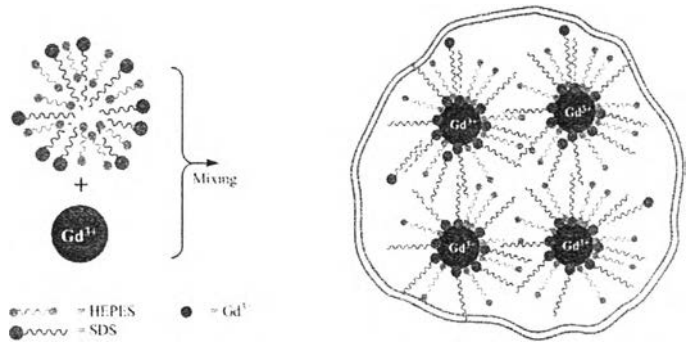


**Scheme 4.4** The possible formation mechanism of **GdSH** nanoparticles in the 0.1 M pH 7.4 HEPES buffer solution, which represent a monolayer protected nanoparticles. The number of surfactants and buffers do not represent the real system.

### 4.2.3 The effects of various surfactants and various buffers to the curcumin derivative ($CurBF_2$) encapsulated in CNPs

To verify the loading of **$CurBF_2$** incorparated in various **CNPs**, the supernatant of **$CurBF_2$** after the centrifugation was measured by UV-visible technique. The color and the absorbance band of supernatant were shown in Figures 4.10 and 4.11.

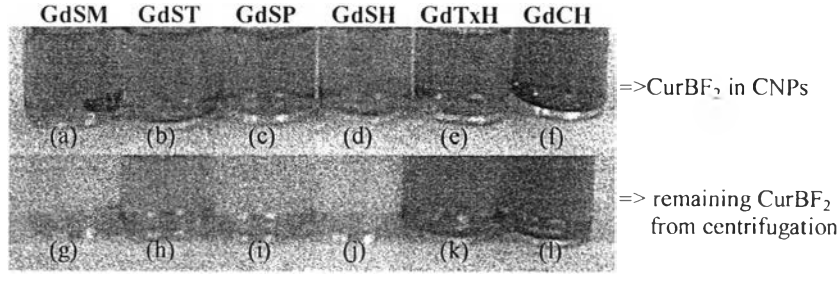


**Figure 4.10** Color changes of **$CurBF_2$** incorporated in **GdSM** (a), **GdST** (b), **GdSP** (c), **GdSH** (d), **GdTH** (e), and **GdCH CNPs** (f) and supernatants of **$CurBF_2$** after centrifuge at 10000 rpm x 10 min of **GdSM** (f), **GdST** (h), **GdSP** (i), **GdSH** (j), **GdTH** (k), and **GdCH CNPs** (l)

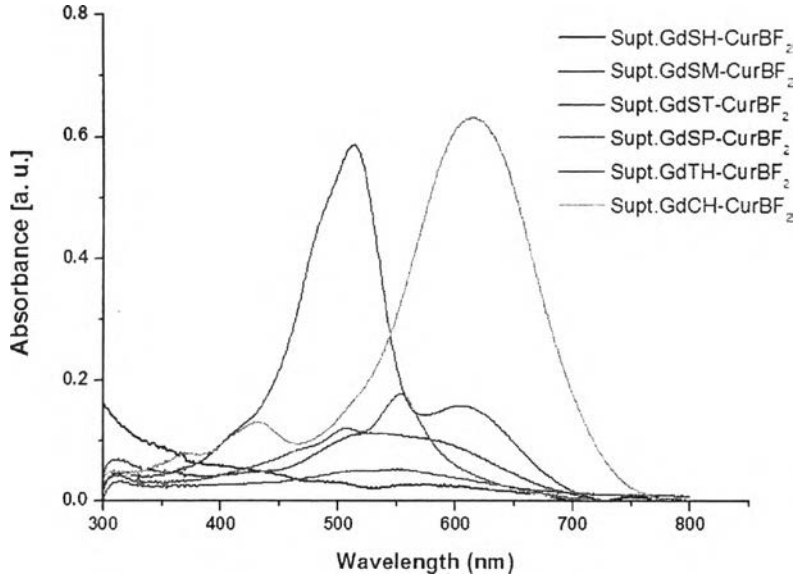


**Figure 4.11** UV-Vis spectra of supernatant of **$CurBF_2$** incorporated in **GdSH**, **GdSM**, **GdST**, **GdSP**, **GdTH** and **GdCH CNPs**

The absorption spectra and color changes of supernatant of **$CurBF_2$** in **GdSH** showed that remaining **$CurBF_2$** in solution were less than those of **$CurBF_2$** in **GdSM**, **GdST**, **GdSP**, **GdTxH** and **GdCH** respectively. The results suggested that **$CurBF_2$** prefers to be encapsulated in **GdSH CNPs** over other **CNPs**. In addition, the strong absortion band of supernatant and FT-IR of **GdTxH** and **GdCH** comfermed that Triton-X and CTAB surfactants formed weak interaction with $Gd^{3+}$ particles, resulting in the formation themselves of residual surfactants in small-size micellar structures.

All results from TEM, DLS, FT-IR and UV-Vis techniques showed a high performance of SDS and HEPES buffer, commonly used in a biological laboratory, as surfactant and co-surfactant, respectively, for the formation of coordination nanoparticles in this system.

### 4.2.4 The effect of various concentrations of SDS surfactant to the curcumin derivative ($CurBF_2$) encapsulated in CNPs

To study the capacity of **$CurBF_2$** encapsulated in **CNPs** by the effect of various concentrations of SDS surfactant, 10 points of SDS concentrations from 0.25 to 5 mM in 0.1 M HEPES buffer solution pH 7.4 were selected in investigation. After the centrifugation of all samples, each supernatant was determined by UV-Vis spectroscopy. Figure 4.12 displayed the absorption spectra of supernatant at the various concentration values.

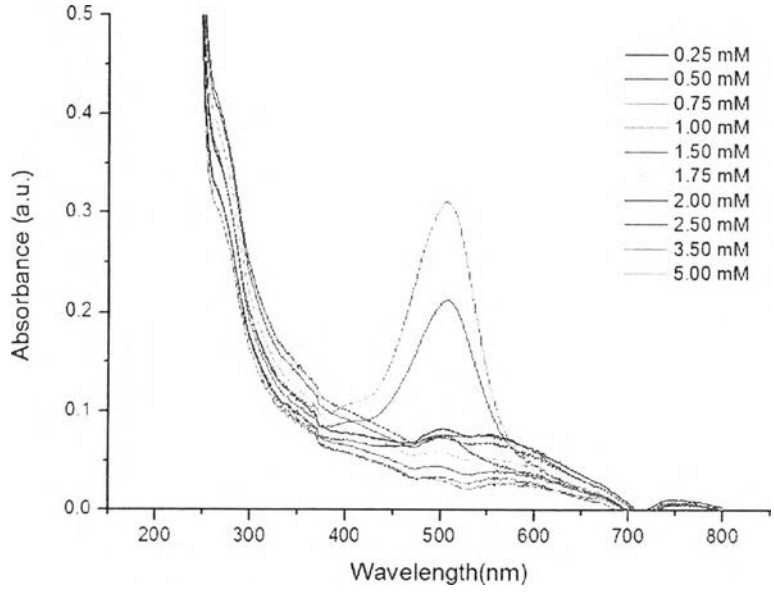


**Figure 4.12** UV-Vis spectra of supernatant after the centrifugation of **GdSH-$CurBF_2$ CNPs** by using SDS at 0.25-5.00 mM in 0.1 M HEPES buffer pH 7.4

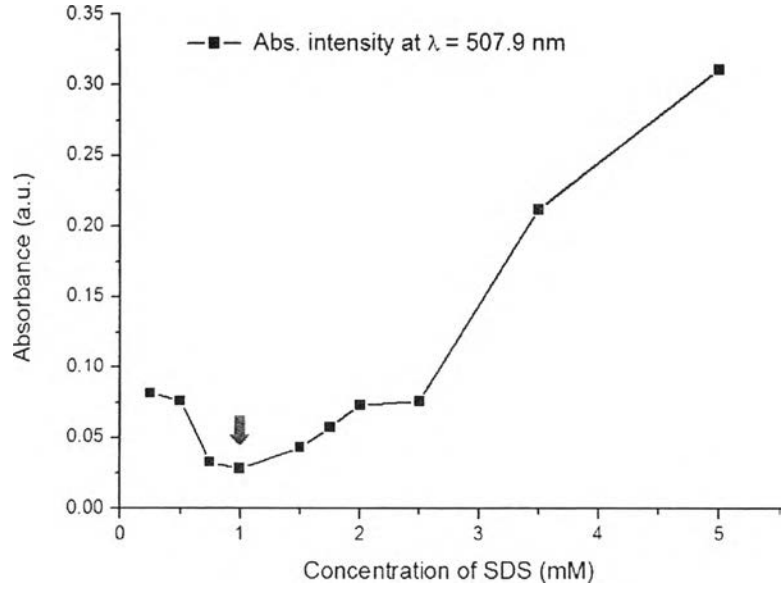


**Figure 4.13** The absorption intensity at $\lambda_{ab}$ = 507.9 nm of supernatant after the centrifugation of **GdSH-CurBF$_2$ CNPs** based on using SDS at 0.25-5.00 mM in 0.1 M HEPES buffer pH 7.4

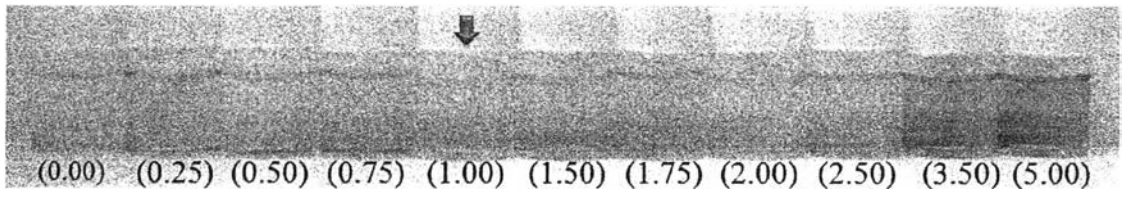


**Figure 4.14** Color changes of the supernatant after the centrifugation of **GdSH-CurBF$_2$ CNPs** based on using SDS at 0.25-5.00 mM in 0.1 M HEPES buffer pH 7.4

Figure 4.13 showed the maximum intensity at $\lambda_{ab}$ = 507.9 nm as a function of SDS concentration. The spectra showed the decrease of the absorbance of curcumin upon the increment of SDS concentration to 1 mM, which is the point that most **CurBF$_2$** could be incorporated in GdSH CNPs. After that the absorbance at 507.9 nm was increased when the concentration of SDS was increased to 5 mM. The color changes of samples with various concentrations were shown in Figure 4.14. The result illustrated that the optimized concentration of SDS for the encapsulation of **CurBF$_2$** in **GdSH CNPs** was 1.00 mM.

### 4.2.5 X-ray absorption near-edge structure (XANES) spectra

To investigate the formation behavior of coordination nanoparticles by $Gd^{3+}$, SDS and HEPES, XAS, ICP-AES and XRD techniques were employed in these experiments. The XAS technique was usually employed to analyze the oxidation state of $Gd^{3+}$ and the binding mode of donor atom based SDS and HEPES for adaptive self-assembled nanoparticles [61]. Gd $L_{III}$ edge XANES spectra showed in Figure 4.15, which was used to characterize the oxidation state of Gd after interaction with the SDS surfactant in HEPES buffer compared with standard materials including Gd foil, $Gd_2O_3$, $Gd(NO_3)_3$ (starting material) and $Gd_2(SO_4)_3$. XANES spectra showed a Gd $L_{III}$ edge of **GdSH CNPs** slightly shift to higher energy from 7247.75 to 7249.01 eV.

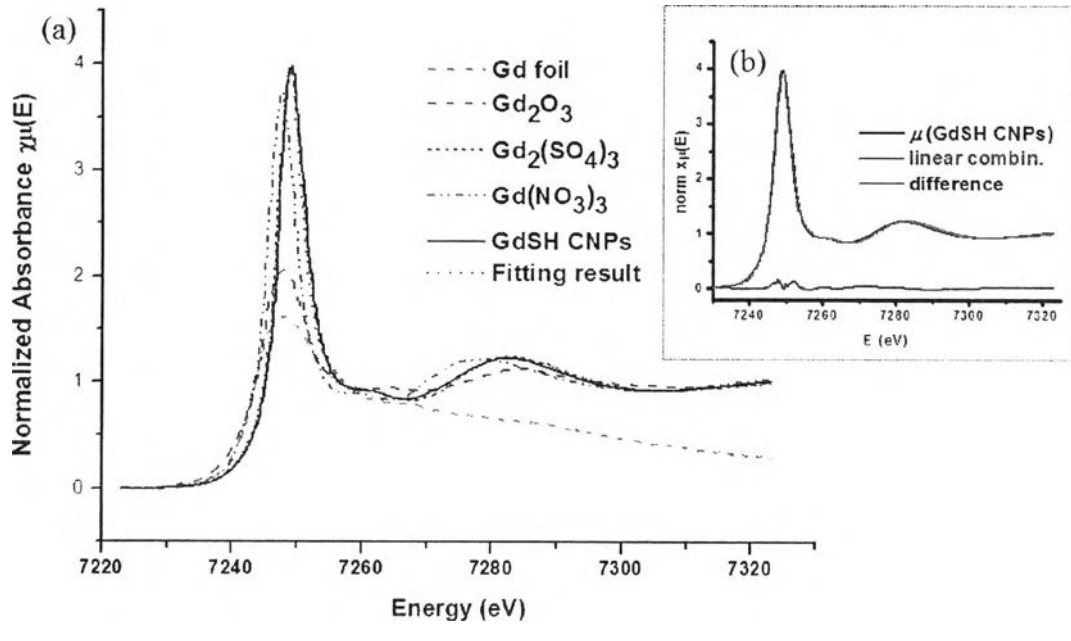


**Figure 4.15** Gd $L_{III}$ edge XANES spectra of sample **GdSH** and reference (a). Linear combination fitting of XANES spectra of Gd (b).

**Table 4.4** Results from linear combination fitting of XANES spectra tool in the Athena Program.

| Compound | $L_{III}$ -edge position *E* (eV) | Weight (%) |
|---|---|---|
| *Sample* | | |
| **GdSH CNPs** | 7249.01 | - |
| *Standard* | | |
| Gd foil | 7247.75 | 0.0 |
| $Gd_2O_3$ | 7247.94 | 0.0 |
| $Gd(NO_3)_3$ | 7247.75 | 9.3 |
| $Gd_2(SO_4)_3$ | 7249.22 | 90.7 |

Linear combination fitting of XANES spectra was calculated by the Athena Program [62,63], which was used to quantify the amount of Gd form in **GdSH CNPs** compared to the XANES data of standard materials as possible compositions. The weight percentage of Gd species was display in Table 4.4. The percentage of Gd in **GdSH CNPs** showed a consistency with $Gd^{3+}$ in $Gd_2(SO_4)_3$ ca. 90.7 %. The XANES results revealed a strong evidence that the oxidation state of gadolinium exists in Gd (III) ion and $Gd^{3+}$ ion interacts with sulfate group. A small shift of the oxidized form of **GdSH CNPs** was possibly stemmed by the interaction of $Gd^{3+}$ with oxygen atom on sulfate group based SDS and HEPES buffer instead of the oxygen atom on nitrate group [63,64]. The $Gd^{3+}$ in the oxidized form in spectrum suggested that $Gd^{3+}$ ion did not be reduced by a nitrogen-centered free radical based HEPES buffer [21].

### 4.2.6 Inductively-coupled plasma atomic emission spectroscopy (ICP-ASE)

ICP-AES was used to quantify the amount of metal ions in the supernatant and to study the binding mode stoichiometry of SDS and HEPES buffer in the novel coordination nanoparticles. The ICP-AES experiment has been utilized to investigate the effects from various SDS in water system and HEPES buffer systems. From Figure 4.16(a), the ratios of [SDS]/[$Gd^{3+}$] from 1 to 5 displayed the decrease of the concentration of $Gd^{3+}$ in supernatant upon the increment of SDS concentration. The decrease of $Gd^{3+}$ concentration was possibly caused by a formation of white precipitate or flocculate found in the sample [59]. The concentration ratios of [SDS]/[$Gd^{3+}$] from 6 to 18 showed the increase of free $Gd^{3+}$ ion in the supernatant. The redissolved precipitate is due to the formation of SDS micelles at the critical micellar concentration of surfactant at around 8 mM [72]. These data were fitted by the Lorentz equation from Origin Pro 8.0 sorfware [73]. Figure 4.16(b) points out that a maximum molar fraction of SDS is 0.75 ± 0.01. It indicated that the stoichiometry of the precipitated form of GdSDS is 3:1 of SDS:$Gd^{3+}$.

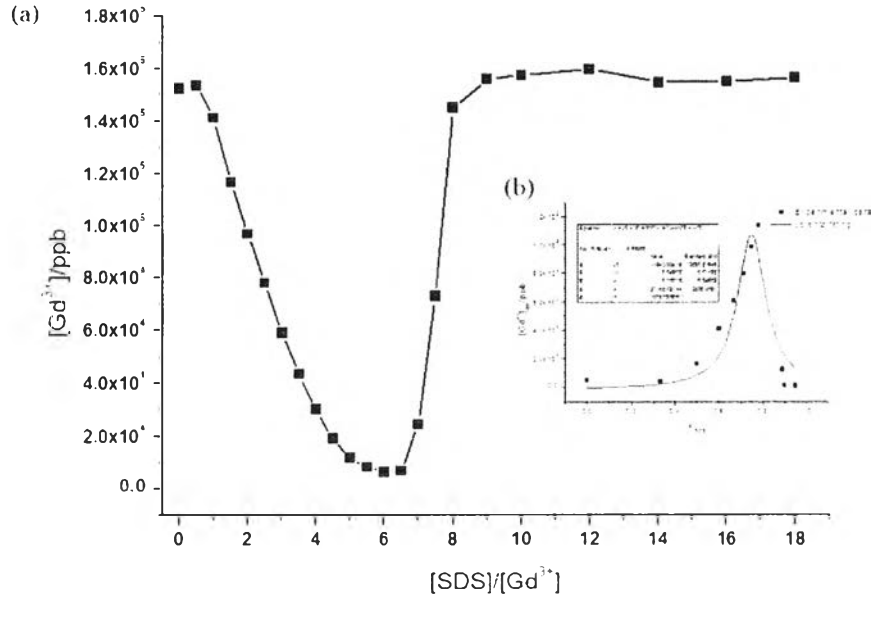


**Figure 4.16** Concentration of $Gd^{3+}$ in supernatant upon various concentration ratios of SDS/$Gd^{3+}$ (0-18 mM) in water (a). The initial concentration of $Gd^{3+}$ was 1 mM. Concentration of $Gd^{3+}$ complex versus the molar fraction of SDS in water (b), the solid line showed the Lorentz equation fitting.

Considering the Figure 4.17, **GdSH CNPs** prepared in 0.1 M HEPES buffer solution pH 7.4 did not form the micelles upon the increment of SDS concentration. In addition, the results from the Lorentz equation in Figure 4.17(b) displayed a maximum molar fraction of SDS in HEPEPS buffer is 0.72 ± 0.01, which gave a stoichiometry of the **CNPs** formation of 2.68:1 ($SDS:Gd^{3+}$). This value was less than that of the precipitated GdSDS. Hence, the HEPES buffer could be corporated with SDS surfactant to form adaptive self-assembled coordination nanoparticles.

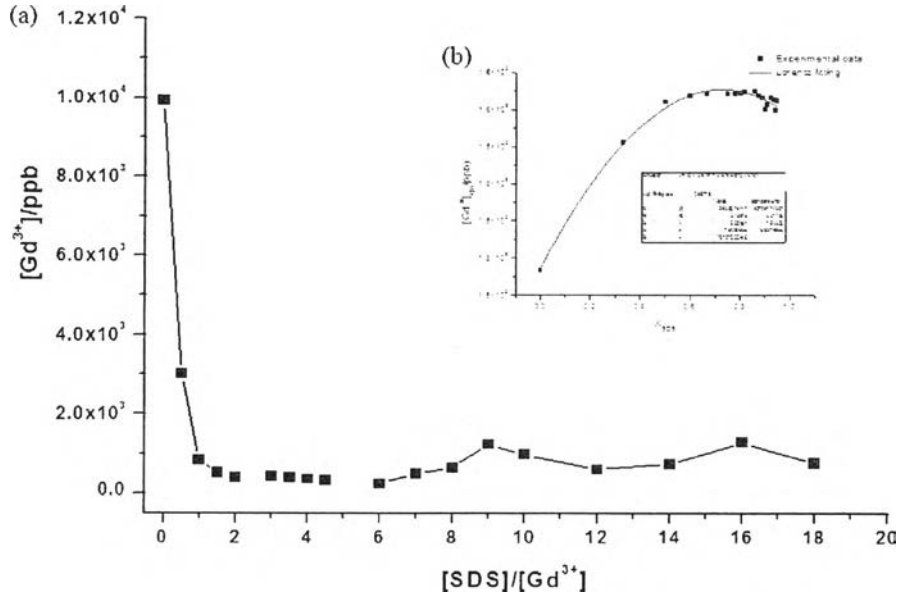


**Figure 4.17** Concentration of $Gd^{3+}$ in supernatant upon various concentration ratios of $SDS/Gd^{3+}$ (0-18 mM) in 0.1 M HEPES buffer pH 7.4 (a). The initial concentration of $Gd^{3+}$ was 1 mM. Concentration of $Gd^{3+}$ complex versus the molar fraction of SDS in HEPES buffer solution (b), the solid line showed the Lorentz equation fitting.

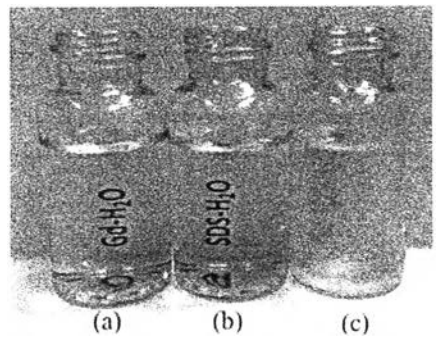


**Figure 4.18** The solubility of the $Gd^{3+}$ (a), SDS surfactant (b) and GdSDS (c) in Milli-Q water

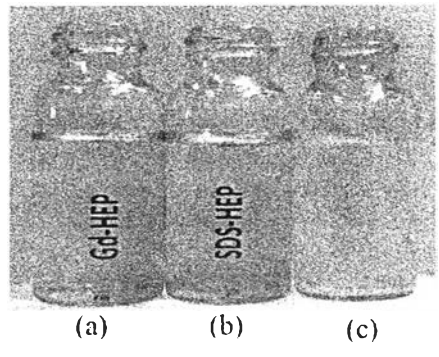


**Figure 4.19** The solubility of the $Gd^{3+}$ (a), SDS surfactant (b) and **GdSH CNPs** (c) in 0.1 M HEPES buffer solution pH 7.4

The solubility of $Gd^{3+}$, SDS and GdSDS (the mixture of $Gd^{3+}$ and SDS) in aqueous solution was shown in Figure 4.18. Each $Gd^{3+}$ and SDS was dissolved in Milli-Q water, which showed clearly solution (Figure 4.18(a-b)), whereas the GdSDS prepared in Milli-Q water demonstrated flocculated aggregates in Figure 4.18(c). The case of $Gd^{3+}$, SDS and **GdSH CNPs** in 0.1 M pH 7.4 HEPES buffer solution was shown in Figure 4.19. The $Gd^{3+}$ and SDS dissolved in HEPES buffer solution showed clearly solution (Figure 4.19(a-b)). Upon the addition of $Gd^{3+}$ in SDS and HEPES buffer solution pH 7.4, the sample **GdSH CNPs** showed milky solution of coordination nanoparticles (Figure 4.19(c)). This suggested that the HEPES buffer performed as a co-surfactant to form the coordination nanoparticles.

### 4.2.7 X-ray Diffraction (XRD)

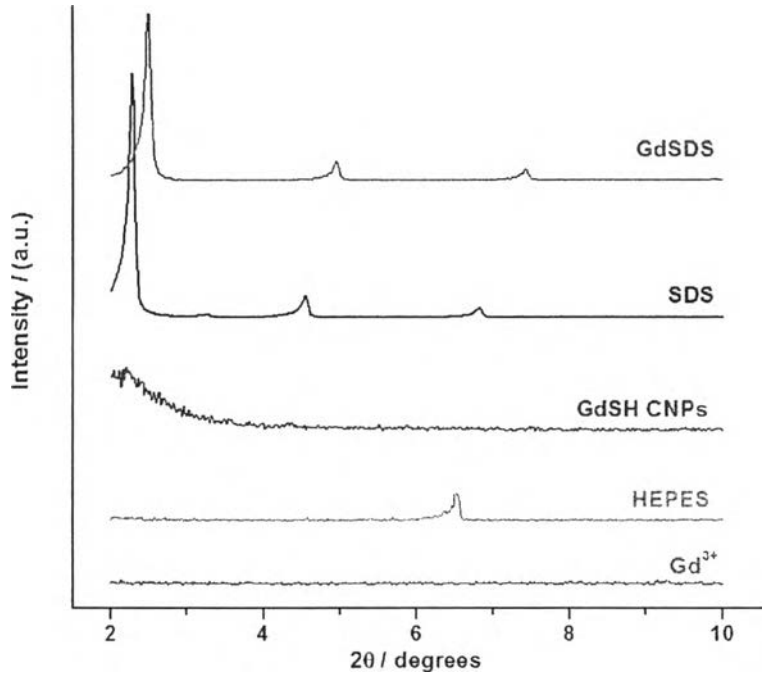


**Figure 4.20** XRD patterns of GdSDS, SDS, **GdSH CNPs**, HEPES and $Gd^{3+}$

Solid state structures of the **GdSH CNPs** and a flocculated GdSDS prepared in HEPEP buffer and water, respectively, were characterized by X-ray power diffraction. X-ray powder diffractograms exhibited at low-angle region (as shown in Figure 4.20) with the characteristic crystalline peaks at $2\theta$ = 2.28, 4.54, 6.82 for SDS and $2\theta$ = 2.50, 4.96, 7.43 for GdSDS, in the attribution of a crystalline characteristic of lamellar arrangement of the flocculated GdSDS [74-75]. In the case of **GdSH CNPs**, the disappearance of all peaks was observed. The pattern showed very low crystallinility. This is indicative of the formation of small crystalline size of coordination nanoparticles [23].

All results from TEM, FTIR, UV-Vis, XAS, ICP-AES and X-ray techniques showed a powerful performance of SDS and HEPES buffer acting possibly as surfactant and co-surfactant, respectively, for the formation of coordination nanoparticles in this system.

### 4.3 Self-assembly of curcumin derivatives encapsulated in GdSH-Cur CNPS

From all results above, we obtained an excellent condition of coordination nanoparticles. To rise the valuable task of the prepared coordination nanoparticle of **GdSH** for biological system, we not only examined the stabilizing roles of **GdSH CNPs** for curcumin derivatives including **curcumin (Cur)**, **$CurBF_2$**, **$CurBF_2OTs$** and **$CurBF_2(OTs)_2$**, but also studied the anti-cancer activity of all CNPs. Free curcumin derivatives were dissolved in 10 % DMSO/ 0.1 M HEPES buffer solution pH 7.4 and the curcumin derivatives encapsulated in **CNPs** were dissolved in 100% 0.1 M HEPES buffer solution pH 7.4 for all manipulations.

#### 4.3.1 Infrared Spectra of curcumin encapsulated in coordination nanoparticles (GdSH-Cur CNPS)

First, the **Cur** loaded in **GdSH CNPs** was characterized by FT-IR spectroscopy.

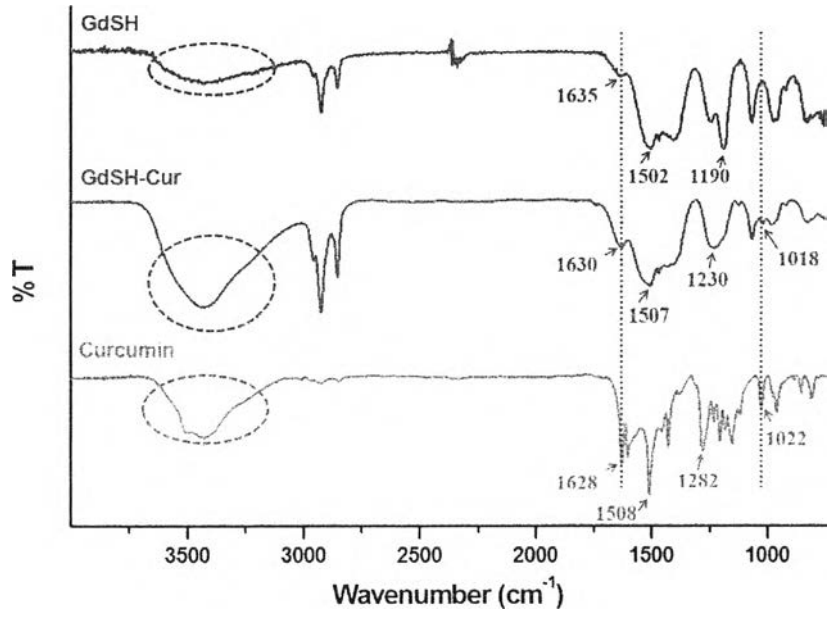


**Figure 4.21** FT-IR spectra of free **Cur**, Cur-containing **GdSH-Cur** and **GdSH CNPs**

A comparison of IR spectra of free **Cur**, **GdSH** and **GdSH-Cur** (Figure 4.21) presented significant changes in the peak shape and the position. The FT-IR spectrum of **Cur** exhibited an absorption band at 3425 $cm^{-1}$ in the attribution of the phenolic O–H stretching vibration, sharp absorption bands at 1603 $cm^{-1}$ (stretching vibrations of benzene ring), 1509 $cm^{-1}$ (C=O and C–C vibrations), 1435 $cm^{-1}$ (olefinic C–H bending vibration) and 1285 $cm^{-1}$ (aromatic C–O stretching vibration) [28]. By reason of the incorporation of **Cur** into the **GdSH-Cur CNPs**, the characteristic peaks of **GdSH-Cur CNPs** presenting a broad peak around 3000-3750 $cm^{-1}$ and the shifts of 1628, 1508 and 1022 $cm^{-1}$ to 1630, 1507 and 1018, respectively, were also observed. These results are indicative of the **Cur** incorporated in the **GdSH CNPs** [76].

### 4.3.2 UV-Vis and fluorescence studies of curcumin encapsulated in coordination nanoparticles (GdSH-Cur CNPs)

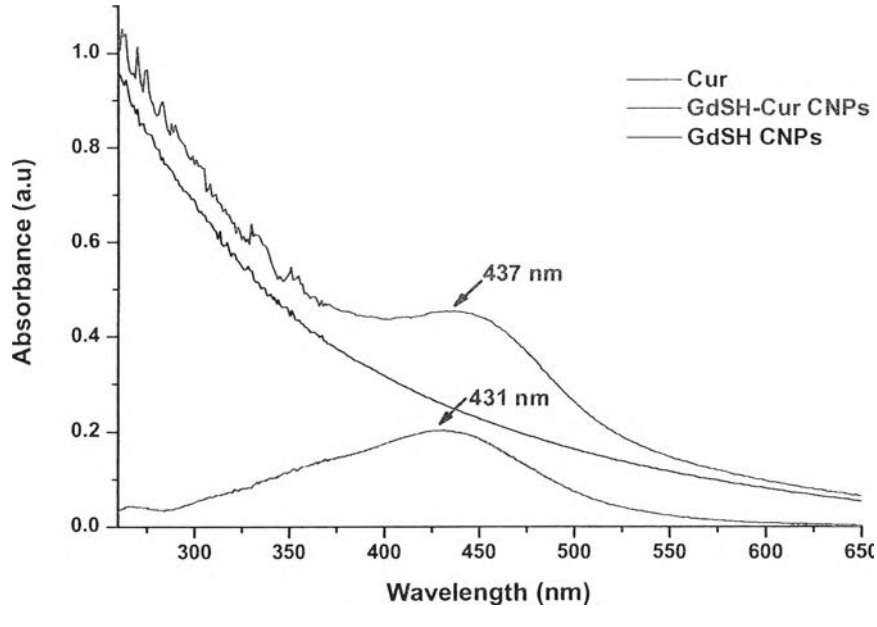


**Figure 4.22** UV-Vis spectra of free **Cur** in 10% DMSO/0.1 M HEPES buffer solution pH 7.4, **GdSH-Cur** and **GdSH CNPs** in 0.1 M HEPES buffer solution pH 7.4

UV-Vis spectra of free **Cur**, **GdSH-Cur** and **GdSH CNPs** were shown in Figure 4.22. The **GdSH-Cur** displayed a red-shift absorption band from 431 to 437 nm. Additionally, the **GdSH-Cur CNPs** exhibited a strong emission band with a concomitant of a blue shift from 553 nm to 532 nm as shown in Figure 4.23. The results indicated that microenvironment of **Cur** was changed after incorporation of

**Cur** into **GdSH CNPs** [9]. All data demonstrated the strong evidences supporting the presence of **Cur** in the **GdSH CNPs**.

Moreover, **Cur** dissolved in aqueous solution showed a weak fluorescence intensity, which was due to the common nonradiative thermal deactivation of singlet excited state. This phenomenon occurred by the free conformational rotation of twistable structure of the keto form of **Cur** leading to an imperfect resonance [38]. Very interestingly, **Cur** incorporated in **CNPs** exposed a strong fluorescence intensity because the **CNPs** can control the conformational rotation of **Cur,** as a result, electron can circulated around a strictly planar molecule of **Cur** [77]. Another reason of the weak fluorescence intensity might be the decomposition of free **Cur** to several fragments under the buffer solution [6]. In the case of **GdSH-Cur CNPs**, **Cur** was prevented from an interactions with the buffer or water molecules by the coordination matrix. The result showed that **GdSH CNPs** could induce the fluorescence enhancement of **Cur** in HEPES buffer solution pH 7.4. This promotes a highly potential task for the fluorescence imaging agents in cell or tissue in the future.

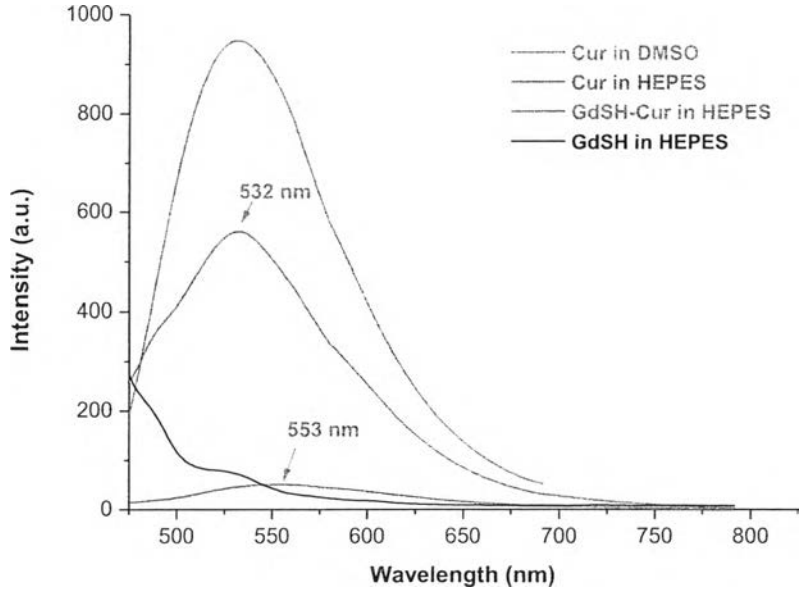


**Figure 4.23** Fluorescence spectra of free **Cur** in DMSO and in 10% DMSO/0.1 M HEPES buffer solution pH 7.4, **GdSH-Cur** and **GdSH CNPs** in 0.1 M HEPES buffer solution pH 7.4 ($\lambda_{ex}$ = 445 nm)

The incorporation of **Cur** in coordination nanoparticles by $Gd^{3+}$/SDS surfactant in HEPES buffer can be explained by the hydrophobic interior formed by

alkyl part of SDS and hydrophobic part of **Cur** or the interaction of OH group and $Gd^{3+}$ [19]. The possible mechanism of the formation of the **curcumin** incorporated in coordination nanoparticles (**GdSH-Cur CNPs**) was shown in Scheme 4.5.

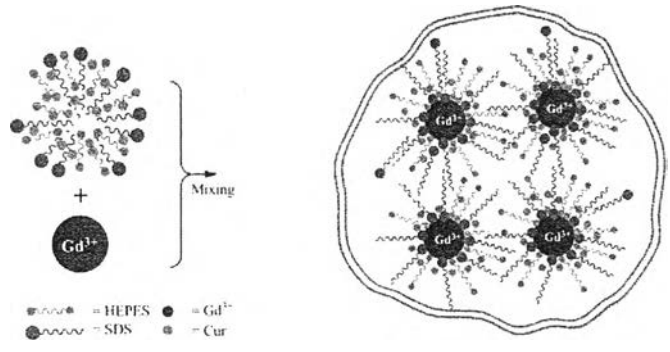


**Scheme 4.5** Postulated formation mechanism of **GdSH-Cur CNPs** in the 0.1 M HEPES buffer solution pH 7.4. The number of surfactants, buffers and **curcumin** do not represent the real system.

### 4.3.3 The stability studies of curcumin encapsulated in coordination nanoparticles (GdSH-Cur CNPs)

It is know that, the curcumin derivatives have been used in fluorescence applications such as imaging agent and cyanide sensor [7,58]. However, the **curcumin** was extremely low solubility and unstable in aqueous solution which was the limitation of bioavailability and clinical efficiency. In this research, we focus on developing the stability of curcumin derivatives by using self-assembled coordination nanoparticles for the biological tasks as imaging agent or drug delivery for cell or tissue in the future.

To study the stability of **Cur** incorporated in **GdSH CNPs**, we employed the fluorescence spectroscopy for determining the fluorescence intensity as a function of time. Figure 4.24 showed the normalized fluorescence intensity at $\lambda_{em}$ of 553 and 532 nm of free **Cur** and **Cur** incorporated in **GdSH CNPs,** respectively, in HEPES buffer solution as a function of time. The normalized fluorescence intensity of free **Cur** was rapidly decreased upon increasing time to 180 min. This implied that free **Cur** was unstable in HEPES buffer solution. In the case of **GdSH-Cur CNPs**, the normalized fluorescence intensity was slowly decreased upon increase of time. The maximum

fluorescence intensity was normalized to a value of 100 at zero time. After 7 days, % normalized intensity of **Cur** and **GdSH-Cur** was 23.36% and 56.92 %, respectively.

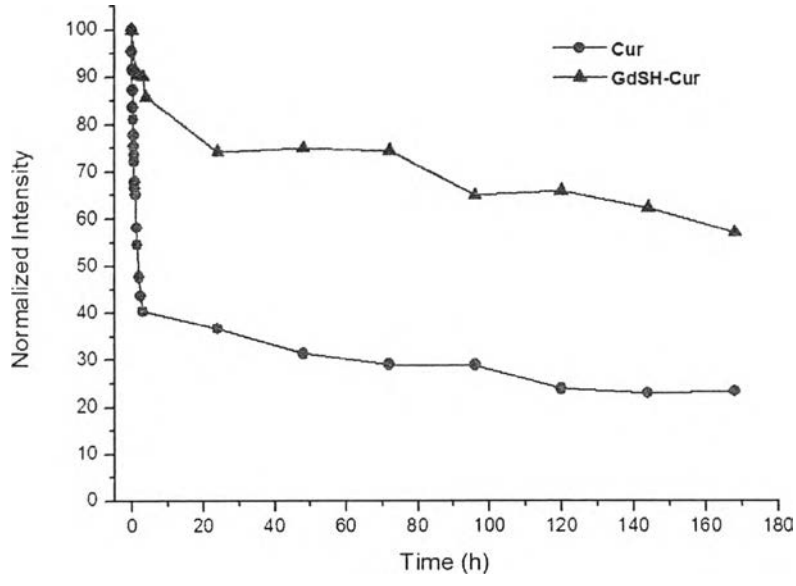


**Figure 4.24** Normalized fluorescence intensity at $\lambda_{em}$ = 553 nm of $1x10^{-5}$ M **Cur** dissolved in 10 % DMSO/0.1 M HEPES buffer solution pH 7.4 and at $\lambda_{em}$ = 532 nm of **GdSH-Cur CNPs** redispersed in 0.1 M HEPES buffer solution pH 7.4. The data were normalized to a value of 100 at zero time.


**Figure 4.25** Color changes of $1x10^{-5}$ M **Cur** dissolved in 10 % DMSO/0.1 M HEPES buffer solution pH 7.4 for 1 min (a) and 240 min (b) and color changes of **GdSH-Cur CNPs** redispersed in 0.1 M HEPES buffer solution pH 7.4 for 1 min (c) and 7 days (d)

Additionally, the color solution of free **Cur**, **GdSH-Cur** dissolved in HEPES buffer solutions upon an increment of time were performed in Figure 4.25(a-d). The yellow solution of free **Cur** in HEPES buffer system was changed to colorless solution within 240 min (as shown in Figure 4.25(b)), whereas the color solution of **curcumin** incorporated in coordination nanoparticle (**GdSH-Cur**) still remained unchanged until 7 days (shown in Figure 4.25(d)). It clearly indicated that the curcumin derivatives incorporated in **GdSH CNPs** were much more stable than those without **GdSH CNPs** in buffer solution.

### 4.3.4 The stability studies of $CurBF_2$ encapsulated in coordination nanoparticles (GdSH-$CurBF_2$ CNPs)

The fluorescence spectra of the **$CurBF_2$** in HEPES buffer solution were shown in Figure 4.26. The spectra displayed the dramatic decrease of fluorescence intensity at $\lambda_{em}$ = 652 and 707 nm and a new peak at $\lambda_{em}$ = 570 nm was developed. This implied that that the **$CurBF_2$** was unstable in HEPES buffer solution. The case of **$CurBF_2$** incorporated in coordination nanoparticles (**GdSH-$CurBF_2$**) presented a slow decrease of the fluorescence intensity at $\lambda_{em}$ = 653 nm as shown in Figure 4.27.

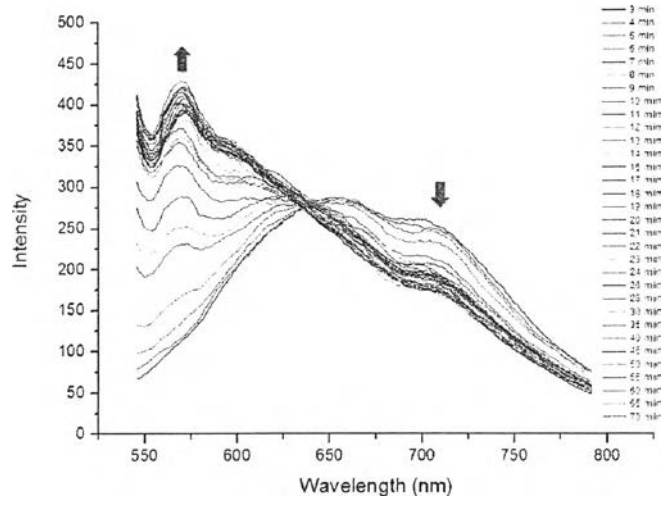


**Figure 4.26** Fluorescence spectra of $1x10^{-5}$ M **$CurBF_2$** in 10% DMSO/0.1 M HEPES buffer solution pH 7.4 from 0 to 70 min, at $\lambda_{ex}$ = 517 nm, slit = 10, pmt = 800

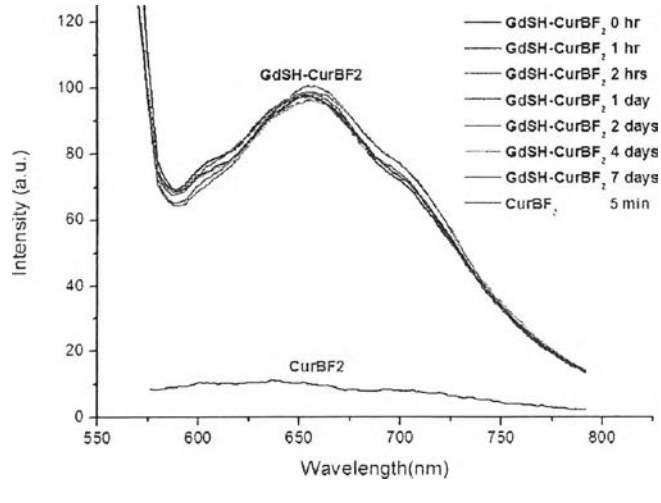


**Figure 4.27** Fluorescence spectra of **GdSH-$CurBF_2$ CNPs** dissolved in 0.1 M HEPES buffer solution pH 7.4 from 0 to 7 days, at $\lambda_{ex}$ = 517 nm, slit = 10, pmt = 700

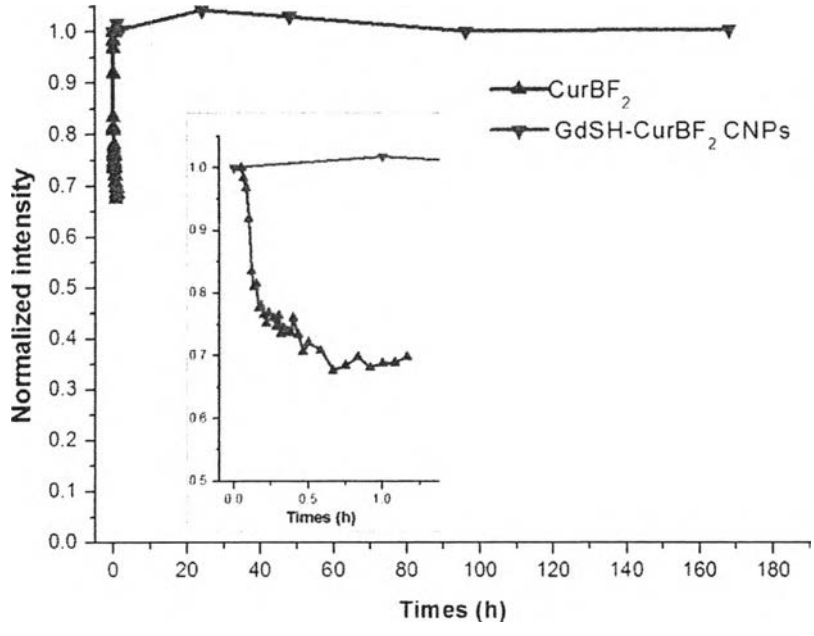


**Figure 4.28** Normalized fluorescence intensity at $\lambda_{em}$ = 707 nm of $1x10^{-5}$ M **$CurBF_2$** dissolved in 10 % DMSO/0.1 M HEPES buffer solution pH 7.4 and at $\lambda_{em}$ = 653 nm of **GdSH-$CurBF_2$ CNPs** redispersed in 0.1 M HEPES buffer solution pH 7.4. Inset picture showed normalized fluorescence intensity from 0-70 min. The data were normalized to a value of 100 at zero time.

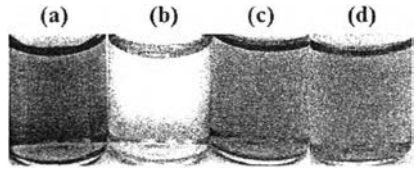


**Figure 4.29** Color solution of $1x10^{-5}$ M **$CurBF_2$** dissolved in 10 % DMSO/0.1 M HEPES buffer solution pH 7.4 for 1 min (a) and 70 min (b) and color solution of **GdSH-$CurBF_2$ CNPs** redispersed in 0.1 M HEPES buffer solution pH 7.4 for 1 min (c) and 7 days (d)

Figure 4.28 showed the normalized intensity curves of **$CurBF_2$** and **GdSH-$CurBF_2$ CNPs** as a function of time. In comparison with the normalized fluorescence intensity curves of **GdSH-$CurBF_2$ CNPs**, the curve in the case of free **$CurBF_2$** was more rapidly decreased. Furthermore, color solution of free **$CurBF_2$** and **GdSH-$CurBF_2$ CNPs** dissolved in HEPES buffer solutions were shown in Figure 4.29(a-d). The blue solution of **$CurBF_2$** in HEPES buffer system changed to colorless solution within 70 min (Figure 4.29(b)). The purple color of **GdSH-$CurBF_2$ CNPs** still remained unchanged in 7 days as shown in Figure 4.29(d). It clearly indicated that the

curcumin derivatives incorporated in **GdSH CNPs** were much more stable than those without incorporated in **GdSH CNPs**. In addition, **GdSH-CurBF$_2$ CNPs** were more stable than **GdSH-Cur CNPs** in buffer solution. Actually, compound **CurBF$_2$** is much more stable than compound **Cur** because **BF$_2$** moiety inhibited the tautomerization of ketone and enol forms [58].

### 4.3.5 The stability studies of CurBF$_2$OTs encapsulated in coordination nanoparticles (GdSH-CurBF$_2$OTs CNPs)

The stability of **CurBF$_2$OTs** was examined by UV-Vis technique. Since the fluorescence spectra of **GdSH-CurBF$_2$OTs** showed very low intensity as shown in Figure 4.30.

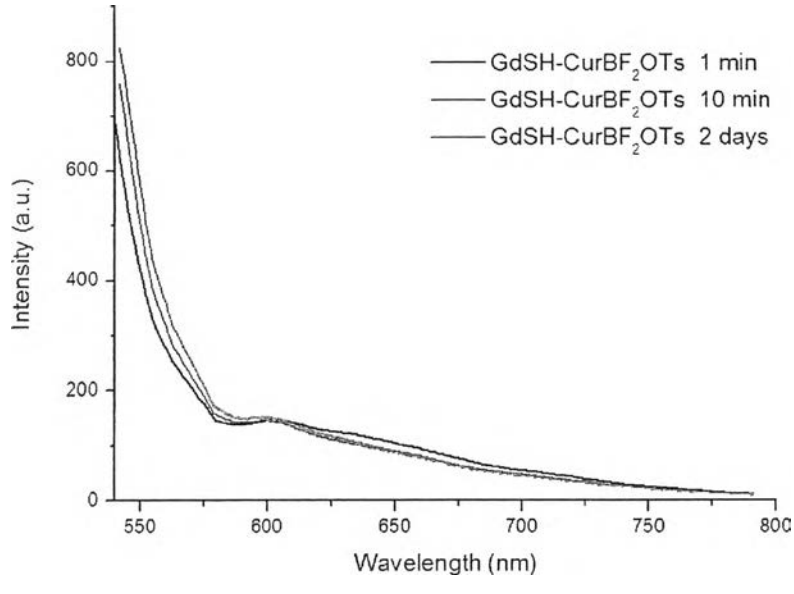


**Figure 4.30** Fluorescence spectra of 1x10$^{-5}$ M **GdSH-CurBF$_2$OTs** in 0.1 M HEPES buffer solution pH 7.4 for 1, 10 min and 2 days at $\lambda_{ex}$ = 506 nm

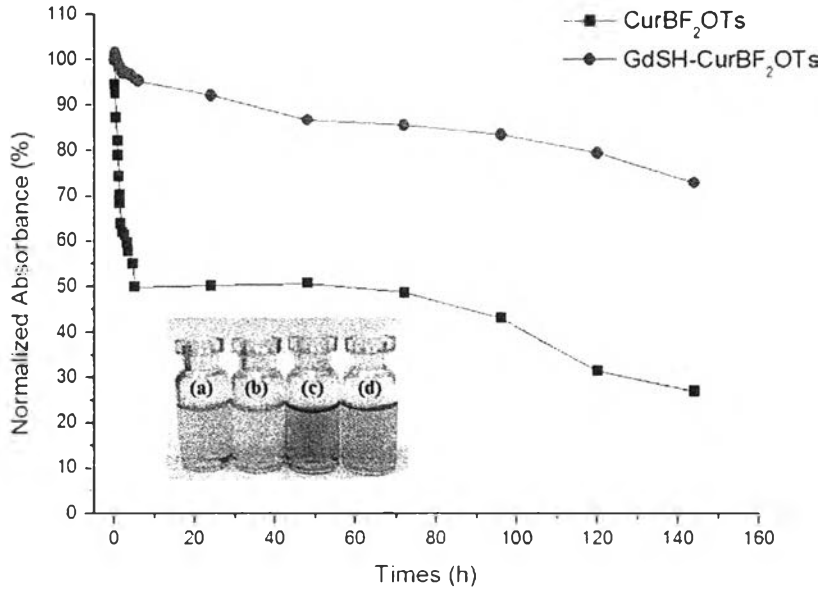


**Figure 4.31** Normalized absorbance at $\lambda_{ab}$ = 464 nm of $1x10^{-5}$ M free **$CurBF_2OTs$** in 10 % DMSO/0.1 M HEPES buffer solution pH 7.4 and at $\lambda_{ab}$ = 509 nm of **GdSH-$CurBF_2OTs$ CNPs** redispersed in 0.1 M HEPES buffer solution pH 7.4 The data were normalized to a value of 100 at zero time. Inset picture showed color solution of $1x10^{-5}$ M free **$CurBF_2OTs$** dissolved in 10 % DMSO/0.1 M HEPES buffer solution pH 7.4 for 1 min (a) and 6 days (b) and color solution of **GdSH-$CurBF_2OTs$ CNPs** redispersed in 0.1 M HEPES buffer solution pH 7.4 for 1 min (c) and 6 days (d)

Figure 4.31 showed dramatic decrease of normalized intensity at $\lambda_{ab}$ = 464 nm for **$CurBF_2OTs$** in HEPES buffer solution as a function of time. The case of **$CurBF_2OTs$** incorporated in coordination nanoparticles presented a slow decrease of normalized intensity at $\lambda_{ab}$ = 509 nm. After 6 days, % normalized intensity of **$CurBF_2OTs$** and **GdSH-$CurBF_2OTs$** was 27.12 % and 73.12 %, respectively.

The color solution of **$CurBF_2OTs$** dissolved in HEPES buffer solution pH 7.4 upon an increment of time were demonstrated in inset of Figure 4.31(a-d). The yellow solution of free **$CurBF_2OTs$** in HEPES buffer system was changed to colorless solution within 6 days (Figure 4.31(b)). The purple colors of **GdSH-$CurBF_2OTs$** remained unchanged even in 7 days as shown in Figure 4.31(d). This reveals that **$CurBF_2OTs$** would be more stable in coordination nanoparticles.

### 4.3.6 The stability studies of $CurBF_2(OTs)_2$ encapsulated in coordination nanoparticles ($GdSH\text{-}CurBF_2(OTs)_2$ CNPs)

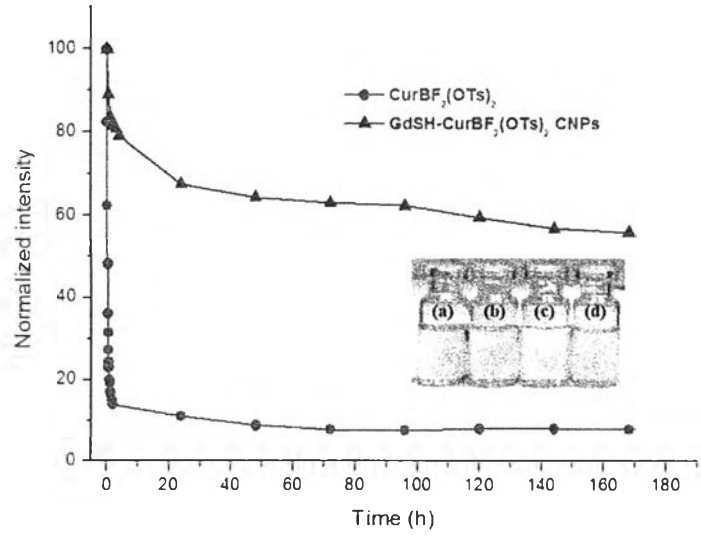


**Figure 4.32** Normalized intensity at $\lambda_{em}$ = 614 nm of $1x10^{-5}$ M **$CurBF_2(OTs)_2$** dissolved in 10 % DMSO/0.1 M HEPES buffer solution pH 7.4 and at $\lambda_{em}$ = 605 nm of **$GdSH\text{-}CurBF_2(OTs)_2$ CNPs** redispersed in 0.1 M HEPES buffer solution pH 7.4. The data were normalized to a value of 100 at zero time. Inset picture showed color solution of $1x10^{-5}$ M **$CurBF_2(OTs)_2$** dissolved in DMSO for 1 min (a), in 10 % DMSO/0.1 M HEPES buffer solution pH 7.4 for 1 min (b) and 240 min (c), and color solution of **$GdSH\text{-}CurBF_2(OTs)_2$ CNPs** in 0.1 M HEPES buffer solution pH 7.4 for 240 min (d).

The stability of **$CurBF_2(OTs)_2$** was examined by fluorescence technique showing a dramatic decrease of normalized intensity at $\lambda_{em}$ = 614 in HEPES buffer pH 7.4 solution as shown in Figure 4.32. The case of **$CurBF_2(OTs)_2$** incorporated in coordination nanoparticles (**$GdSH\text{-}CurBF_2(OTs)_2$**) presented a slow decrease of normalized intensity at $\lambda_{em}$ = 605 nm. After 7 days, % normalized intensity of **$CurBF_2(OTs)_2$** and **$GdSH\text{-}CurBF_2(OTs)_2$** was 7.97 % and 55.82 %, respectively. The color solution of **$CurBF_2(OTs)_2$** in DMSO and HEPES buffer solution were shown in inset of Figure 4.32(a-d). The yellow solution of free **$CurBF_2(OTs)_2$** in HEPES buffer system was changed to colorless solution within 240 min (Figure 4.32(c)) while the yellow solution of **$GdSH\text{-}CurBF_2(OTs)_2$** still remained unchanged within 240 min as shown in Figure 4.32(d). As the results of optical changes, curcumin derivatives incorporated in the coordination nanoparticles of **GdSH** are more stable than those non-corporated in the **GdSH CNPs**.

### 4.3.7 Entrapment efficiency and loading efficiency

Loading efficiency (%) and entrapment efficiency (%) of curcumin derivatives incorporated in coordination nanoparticle were calculated by using equation (1) and (2). The Table 4.5 showed the increase of loading efficiency (%) upon the increment of the concentration of **Cur** in **GdSH-Cur CNPs**. It was implied that the coordination nanoparticle could encapsulate the curcumin derivatives by the electrostatic interaction of $Gd^{3+}$ and hydroxyl group based curcumin and the complementary hydrophobic interaction between alkyl part of SDS and **curcumin**.

**Table 4.5** Loading efficiency (%) and entrapment efficiency (%) of curcumin derivatives calculated by using equation (1) and (2)

| Samples name | Curcumin derivatives concentration (M) | Loading efficiency (%) | Entrapment efficiency (%) |
|---|---|---|---|
| **GdSH-Cur** | $1x10^{-4}$ | 4.98 | 97.97 |
| **GdSH-Cur** | $1x10^{-5}$ | 0.61 | 94.66 |
| **GdSH-CurBF$_2$** | $1x10^{-5}$ | 0.63 | 92.99 |
| **GdSH-CurBF$_2$(OTs)** | $1x10^{-5}$ | 0.64 | 91.55 |
| **GdSH-CurBF$_2$(OTS)$_2$** | $1x10^{-5}$ | 0.62 | 88.78 |

### 4.3.8 Drug release studies

Actaully, the microenvironment of several cancer cells was more acidic than normal tissues with the pH ranged from 5.6 to 7.6 and 7.2 to 7.6, respectively [78]. Our hypothesis about drug release of these nanoparticles is the pH dependence. The investigation of drug release was carried out at pH 6.5 and 7.4 of 0.1 M HEPES buffer solution. The quantification of **curcumin** release was determined by UV-Visible spectrophotometry and calculated by equation (3) [7]. The drug release from **CNPs** matrix upon increasing the time was displayed in Figure 4.33. The % **curcumin** release from **CNPs** matrix is 71.89% and 69.33 % at pH 6.5 and 7.4, respectively, at 4 days. The pH-dependent drug release can be explained that the sulfonate anion of HEPES would be protonated at pH 6.4. Consequently, the coordination nanoparticles were destroyed and **curcumin** was easily removed from coordination nanoparticles as illustrated in Scheme 4.6. [79,80].

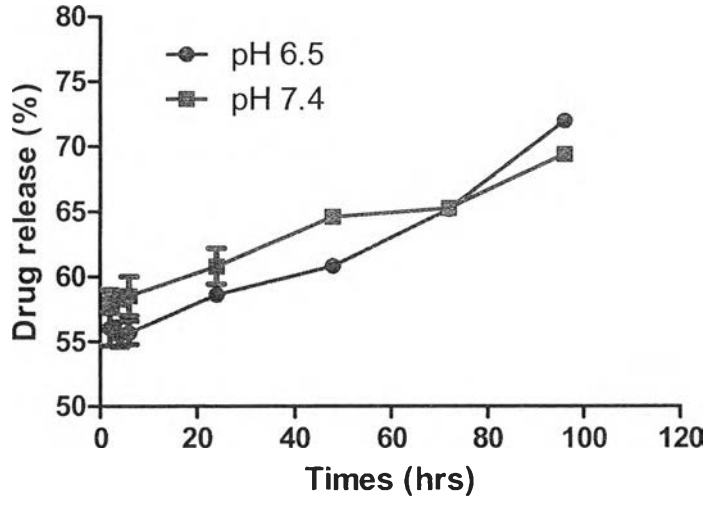


**Figure 4.33** Drug release of **curcumin** from **GdSH CNPs** in HEPES buffer solution pH 6.5 and 7.4 for 2, 4, 6, 24, 48, 72, 96 h

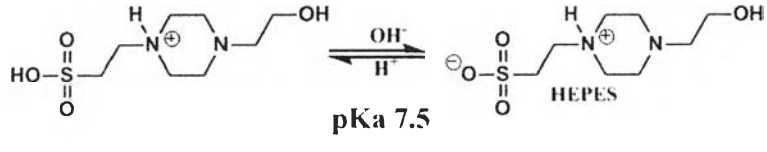


**Scheme 4.6** Dissociation mechanism of HEPES at pKa 7.5 [79]

### 4.4 Cytotoxicity assay

As widely known, the **curcumin** is of great interest for an anti-cancer agent by inducing apoptosis [42]. To investigate the anti-cancer efficiency of curcumin derivatives including **Cur**, **$CurBF_2$**, **$CurBF_2OTs$** and **$CurBF_2(OTs)_2$**, all of compounds were dissolved in DMSO, then the solutions were mixed with the cell culture media. Cytotoxicity of SW620 cancer cells with 4 cucumin derivatives was determined by MTT assay.

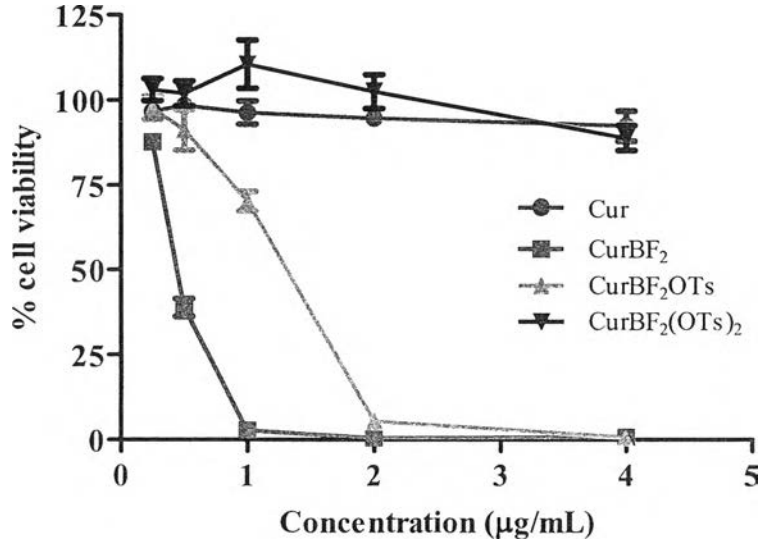


**Figure 4.34** Cell viability of SW620 cancer cells treated with **Cur**, **$CurBF_2$**, **$CurBF_2OTs$** and **$CurBF_2(OTs)_2$** in range of 0.25-4 μg/ml (in DMSO with the cell culture media) for 4 days.

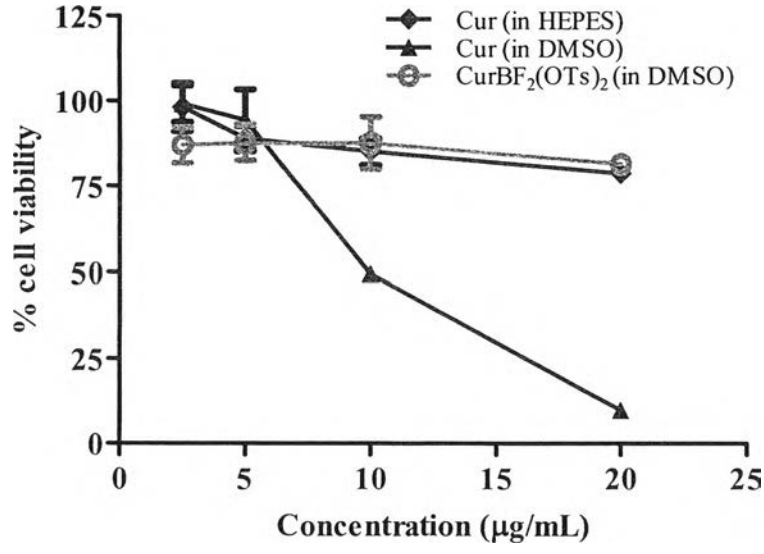


**Figure 4.35** Cell viability of SW620 cancer cells treated with **Cur** (in DMSO and 0.1 M HEPES buffer solution pH 7.4 with the cell culture media ) and **$CurBF_2(OTs)_2$** (in DMSO with the cell culture media) in range of 2.5-20 μg/ml for 4 days.

Figure 4.34-4.35 demonstrated that, the anti-cancer study of **$CurBF_2$** showed more efficiency than **$CurBF_2OTs$**, **Cur** and **$CurBF_2(OTs)_2$**, respectively. Possibly, the coordination of **$BF_2$** could encourage the planarity structure of **Cur** inducing in a high delocalization on molecule and increasing a stability of compund. This approach could improve an anti-cancer efficiency. Interestingly, when a hydroxyl group was replaced by a tosyl group, the anti-cancer efficiency of compound was decreased. Hence, it was implied that the hydroxyl group of curcumin derivatives is one important factor for an anti-cancer efficiency. In the next experiment, we selected the **Cur** and **$CurBF_2$** to study an anti-cancer efficiency. The comparison of anti-cancer tasks of dyes with and without coordination nanoparticles was investigated.

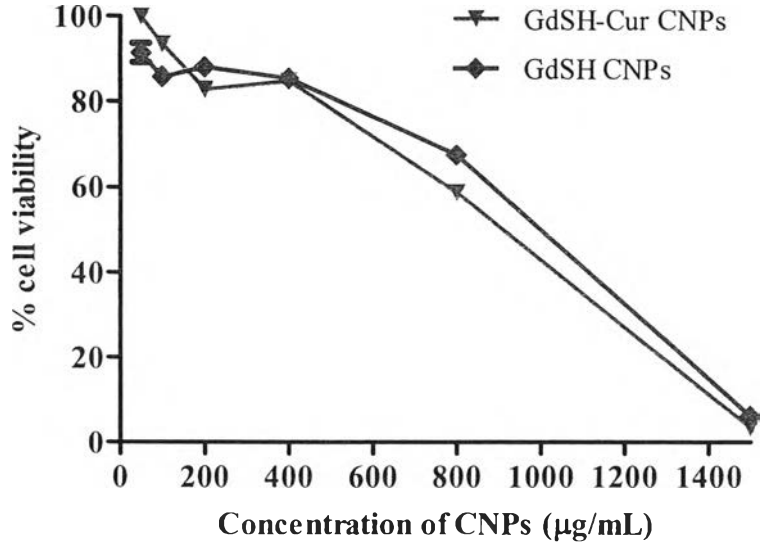


**Figure 4.36** Cell viability of SW620 cancer cells treated with **GdSH-Cur CNPs** and **GdSH CNPs** in range of 50-1500 µg/ml dissolved in 0.1 M HEPES buffer solution pH 7.4 with the cell culture media, the initial prepared concentration of **curcumin** in **GdSH-Cur CNPs** was $10x10^{-5}$ M.

To verify the proper concentration of **GdSH CNPs** and **GdSH-Cur CNPs** towards the anti-cancer activity, various concentration of **GdSH CNPs** and **GdSH-Cur CNPs**, with the initial concentration of **Cur** at $1x10^{-5}$ M, in range of 0-1400 µg/mL showed the % cell viability in Figure 4.36. From the cell viability curve, **GdSH CNPs** with and without Cur showed similar activities. This implied that **GdSH CNPs** with and without **Cur** showed a toxicity to cancer cell with a high concentration of **CNPs**. Interestingly, the concentration of **CNPs** in range of 0-400 µg/mL gave a low influence on the SW620 cancer cell. To avoid the direct interference of **GdSH CNPs** toward cancer cell, we should increase the initial concentration of **Cur** in order to increase % Entrapment of **Cur** in **CNPs** and the use of **GdSH CNPs** concentration is less than 400 µg/mL. Undoubtedly, the anti-cancer cell by **GdSH CNPs** should be ignored and a higher activity of anti-cancer cell could be clearly claimed by **Cur** incorporated in **GdSH CNPs**. Therefore, for the next experiment about the anti-cancer activity, the initial concentration of **Cur** prepared in **GdSH CNPs** is approximately $1x10^{-4}$ M and the range of **GdSH CNPs** concentration is around 0-400 µg/mL.

Cytotoxicity of L292 normal cells and SW620 cancer cells by **GdSH** and **GdSH-Cur CNPs** in 0.1 M HEPES buffer solution pH 7.4 with the cell culture media was determined by MTT assay.

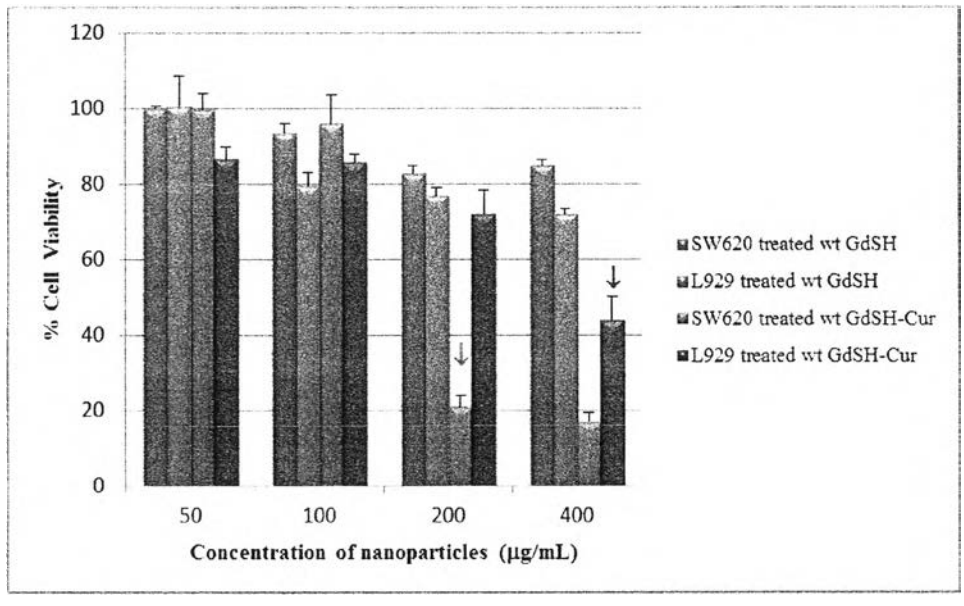


**Figure 4.37** Cell viability of L292 normal cells and SW620 cancer cells treated with **GdSH CNPs** and **GdSH-Cur CNPs** in range of 50-400 µg/ml (dissolved in 0.1 M HEPES buffer solution pH 7.4 with the cell culture media) for 4 days, the initial prepared concentration of **Cur** in **GdSH-Cur CNPs** was $10x10^{-4}$ M.

In Figure 4.37, **GdSH CNPs** showed high cell viability of L292 and SW620 cells in concentration range of 50-400 µg/mL after treated 4 days. The approximately 80% cell viability demonstrated that the samples were non-toxic to the L292 and SW620 cells [7]. The case of the **GdSH-Cur CNPs** exhibited very low cell viability of the SW620 when exposed to the concentration of **GdSH-Cur CNPs** in 200 µg/mL. This indicated that the cytotoxicity of tumor cell in the presence of **GdSH-Cur CNPs** is possibly caused by curcumin. The **GdSH-Cur CNPs** showed non-toxicity to L292 at the same concentration. For 400 µg/mL of **GdSH-Cur CNPs,** a significant toxicity to L292 cells is possibly due to the combination of toxicity from **Cur** and **GdSH CNPs** in **GdSH-Cur CNPs** at high concentration. However, the **GdSH-Cur CNPs** performed the toxicity to L292 normal cell. The proper concentration of nanoparticles for anti-cancer cell should be 200 µg/mL, which give a low toxicity toward a normal cells and a high toxicity to the cancer cells. As our proposed concept, the **GdSH-Cur CNPs** with the particles size of 157.67 nm were especially delivered to the cancer cells more than other tissues by the phenomena of enhancing permeability and retention effect (EPR effect) [15-17].

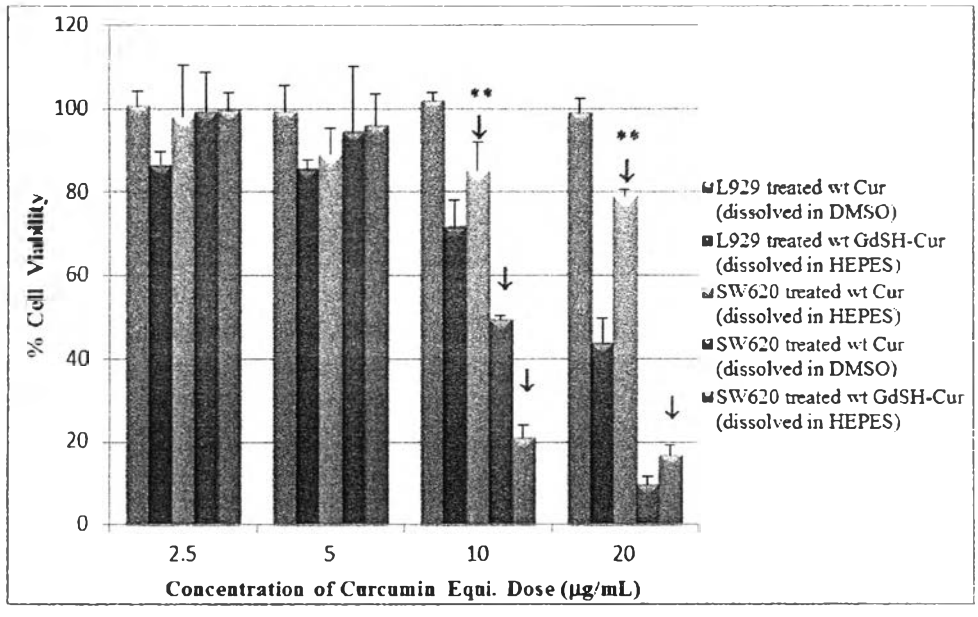


**Figure 4.38** Cell viability of L292 normal cells and SW620 cancer cells treated with **GdSH-Cur CNPs** (dissolved in 0.1 M HEPES buffer solution pH 7.4 with the cell culture media) and their **Cur** equivalent dose in range of 2.5-20 µg/ml (dissolved in DMSO and 0.1 M HEPES buffer solution pH 7.4 with the cell culture media) for 4 days.

Data displayed a mean ± standard derivation, n = 3 and (**) represented that the differences of statistically significant at $p$-value < 0.05.

From Figure 4.38, the L929 and SW620 cells after treated with **Cur** (dissolved in DMSO or HEPES) and **GdSH-Cur CNPs** (dissolved in HEPES) for 4 days showed high cell viability in concentration range of 2.5-5 µg/mL, implying that these concentration range of samples showed non-toxicity to L929 cell and SW620. In the case of the concentration of 10-20 µg/mL, the **Cur** dissolved in DMSO increased the toxicity to SW620 cells, but non-toxicity to L929 cells. The case of **GdSH-Cur CNPs** showed the increase of toxicity to both L929 and SW620 cell. On the other hand, **GdSH-Cur CNPs** not only exhibit the toxicity to the SW620 cancer cells more than the L929 normal cells, but also showed the toxicity to SW620 cells more than free **Cur** did (dissolved in both DMSO and HEPES). In particular of the concentration of **curcumin** equivalence dose 10 µg/mL, the effect of anti-cancer of **GdSH-Cur CNPs** to SW620 cells was significantly higher than that of anti-cancer of free **Cur** dissolved in DMSO and HEPES buffer solution ($p$-value<0.05) [65,66]. From the Table 4.6, the **GdSH-Cur CNPs** dissolved in HEPES displayed higher cytotoxicity to SW620 cancer cells than **Cur** dissolved in DMSO and HEPES buffer with $IC_{50\text{-}Ceq}$ values = 8.03, 10.30 µg/mL and non-toxicity, respectively.

**Table 4.6** The $IC_{50}$ values towards L929 (normal cells) and SW620 (cancer cells) of curcumin derivatives equivalent dose ($IC_{50\text{-}Ceq}$) and coordination nanoparticles ($IC_{50\text{-}CNPs}$), calculated using loading contents

| Entry | $IC_{50\text{-}Ceq}$ (μg/ml) | | $IC_{50\text{-}CNPs}$ (μg/ml) | |
|---|---|---|---|---|
| | L929 cells | SW620 cells | L929 cells | SW620 cells |
| **GdSH** in HEPES | -[a] | -[a] | non-toxic | non-toxic |
| **Cur** in DMSO | non-toxic | 10.30 | -[b] | -[b] |
| **Cur** in HEPES | -[c] | non-toxic | -[b] | -[b] |
| **GdSH-Cur** | 17.80 | 8.03 | 357.40 | 161.2 |
| **$CurBF_2$** in DMSO | 2.04 | 0.83 | -[b] | -[b] |
| **GdSH-$CurBF_2$** | 1.65 | 0.66 | 262.40 | 104.00 |

*Concentration range of curcumin derivatives **CNPs** = 50-400 μg/ml, which was the **Cur** equivalence dose = 2.5-20 μg/ml and **$CurBF_2$** = 0.3125-2.5 μg/ml.
-[a] = no curcumin , $IC_{50\text{-}Ceq}$ cannot be determined
-[b] = no coordination nanoparticles, $IC_{50\text{-}CNPs}$ cannot be determined
-[c] = no experimemt

Cytotoxicity of L929 and SW620 cells by curcumin derivatives in the equivalent dose and **GdSH-Cur CNPs** were determined by MTT assay as shown in Figure 4.38-4.39. The $IC_{50}$ summarized values were shown in Table 4.6. The $IC_{50}$ values of L929 (normal cells) and SW620 (cancer cells) in term of curcumin derivatives equivalent dose ($IC_{50\text{-}Ceq}$) was calculated using loading efficiency of $IC_{50}$ coordination nanoparticles ($IC_{50\text{-}CNPs}$) in the equation of $IC_{50\text{-}Ceq} = IC_{50\text{-}CNPs}$ x loading efficiency /100 [8].

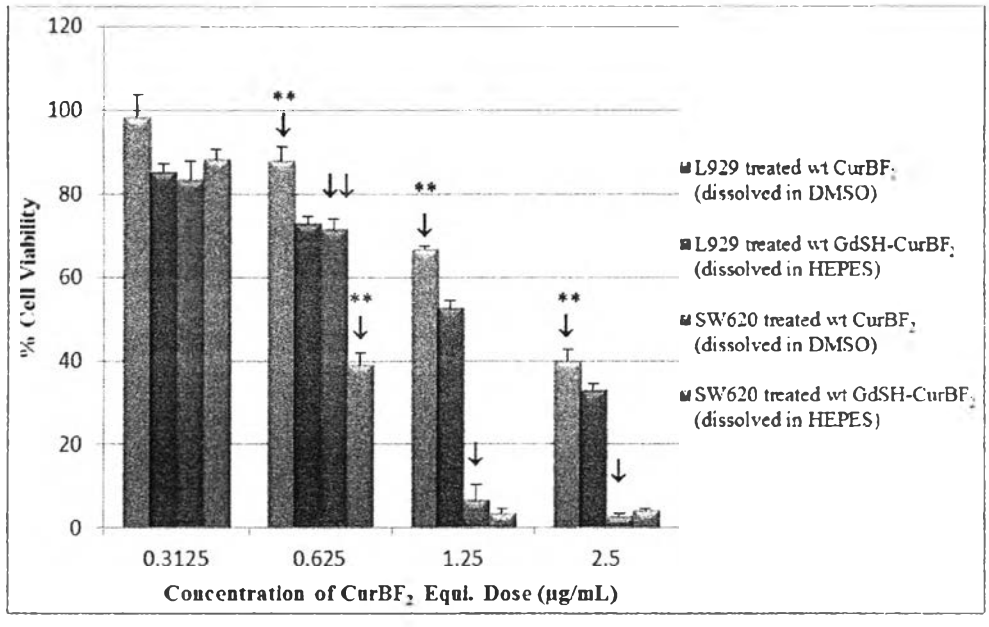


**Figure 4.39** Cell viability of L292 normal cells and SW620 cancer cells treated with **GdSH-CurBF$_2$ CNPs** (dissolved in 0.1 M HEPES buffer solution pH 7.4 with the cell culture media) and their **CurBF$_2$** equivalent dose in range of 0.3125-2.5 µg/ml (dissolved in DMSO with the cell culture media) for 4 days.
Data displayed a mean ± standard derivation, n = 3 and (**) represented that the differences of statistically significant at $p$-value < 0.05.

Considerably, the anti-cancer activity of **CurBF$_2$** was also investigated. In Figure 4.39, the significant % cell viability of L292 normal cells was higher than that of SW620 cancer cells in concentrations range between 0.625-2.5 µg/mL of **CurBF$_2$** (black **), which were a good candidate for the use of an anti-cancer drug in the future work. Furthermore, the effective anti-cancer of **GdSH-CurBF$_2$ CNPs** were significantly higher than that of **CurBF$_2$** (dissolved in DMSO) at the concentration equivalent dose of **CurBF$_2$** at 0.625 µg/mL (red **). From Table 4.6, the **GdSH-CurBF$_2$ CNPs** displayed the highest cytotoxicity to SW620 cancer cells with $IC_{50\text{-}Ceq}$ = 0.66 µg/mL, which was more toxic than the **CurBF$_2$** dissolved in DMSO with $IC_{50\text{-}Ceq}$ = 0.88 µg/mL. Our results demonstrated that **Cur** and **CurBF$_2$** could increase the anti-cancer activity after encapsulated in the coordination nanoparticles.

### 4.5 Cellular uptake of GdSH-Cur CNPs by SW620 cells

Cellular uptake studies of **GdSH-Cur CNPs** were monitored by the visual fluorescence of **curcumin** using florescence microscopy and confocal florescence microscopy. The bright field image and florescence image by using florescence microscopy of controlled SW620 cells were showed in Figure 4.40, which confirmed non-florescence of SW620 cells.

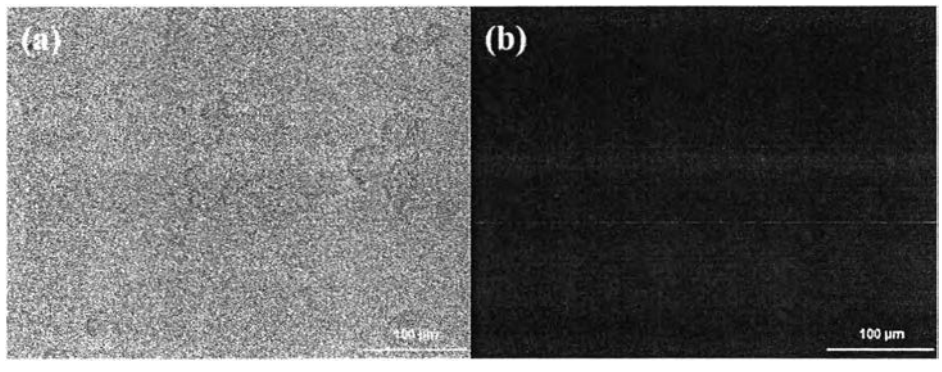


**Figure 4.40** Bright field image (a) and fluorescence image (b) of controlled SW620 cell at 40x incubated with 10% DMSO/RPMI 1640 medium for 24 h.

**Table 4.7** Bright field images and fluorescence images of SW620 at 40x incubated with 10 µg/ml **Cur** in 10% DMSO/0.1 M HEPES buffer solution pH 7.4 (left), 10 µg/ml **curcumin**-equivalent dose of **GdSH-Cur CNPs** (middle) and 25 µg/ml **curcumin**-equivalent dose of **GdSH-Cur CNPs** 0.1 M HEPES buffer solution pH 7.4 (right) for 1, 2, 4, 6, 24 and 48 h.

| Time | 10 µg/mL Cur in 10% DMSO/HEPES | 10 µg/mL GdSH-Cur CNPs in HEPES | 25 µg/mL GdSH-Cur CNPs in HEPES |
|---|---|---|---|
| 1 h | 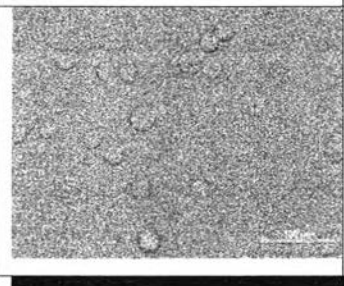 | 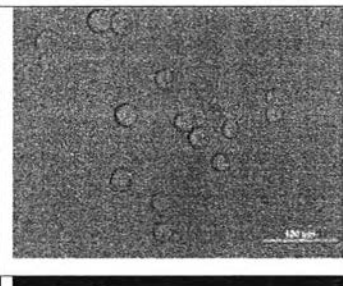 | 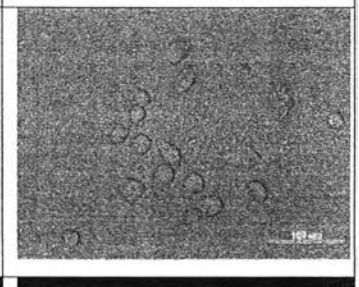 |
| | 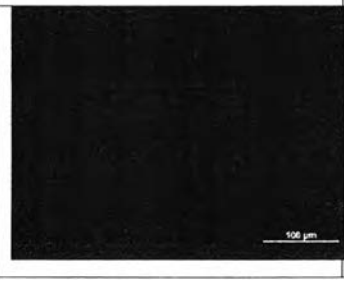 | 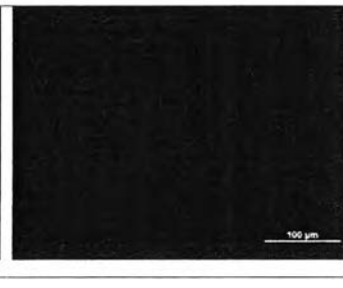 | 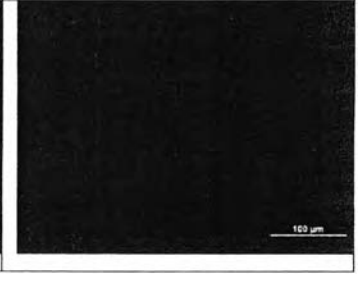 |

| Time | 10 μg/mL Cur in 10% DMSO/HEPES | 10 μg/mL GdSH-Cur CNPs in HEPES | 25 μg/mL GdSH-Cur CNPs in HEPES |
|---|---|---|---|
| 2 h | 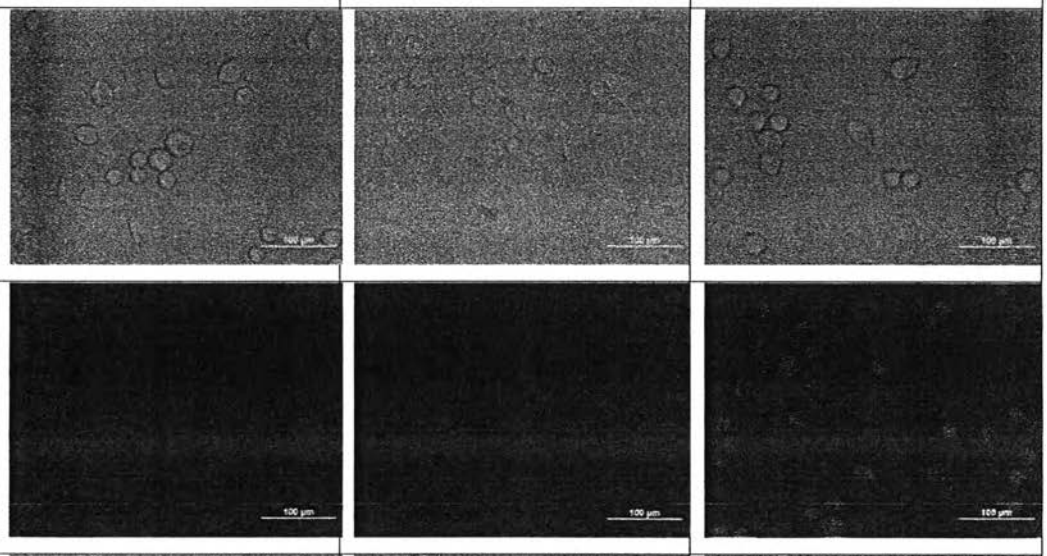 | | |
| 4 h | 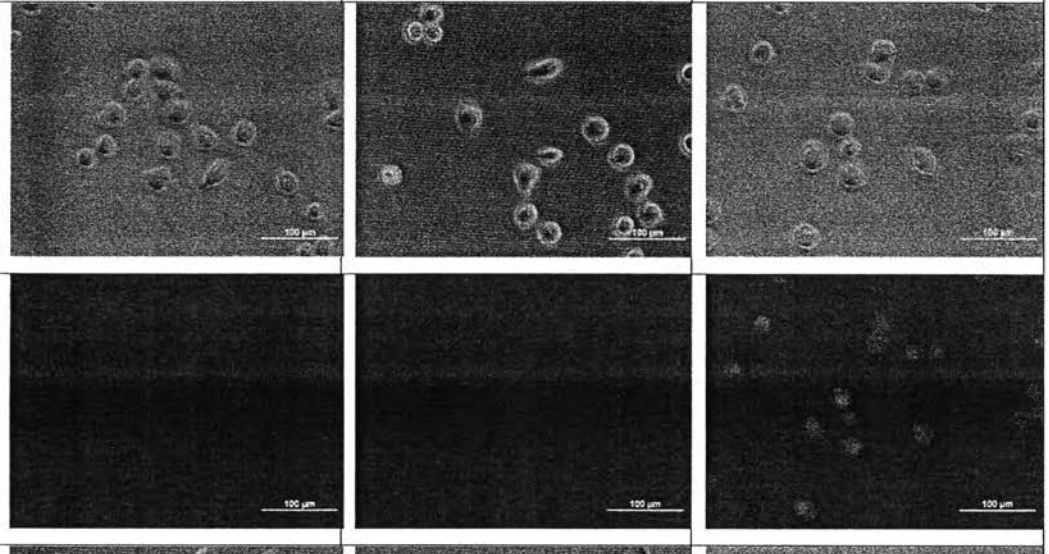 | | |
| 6 h | 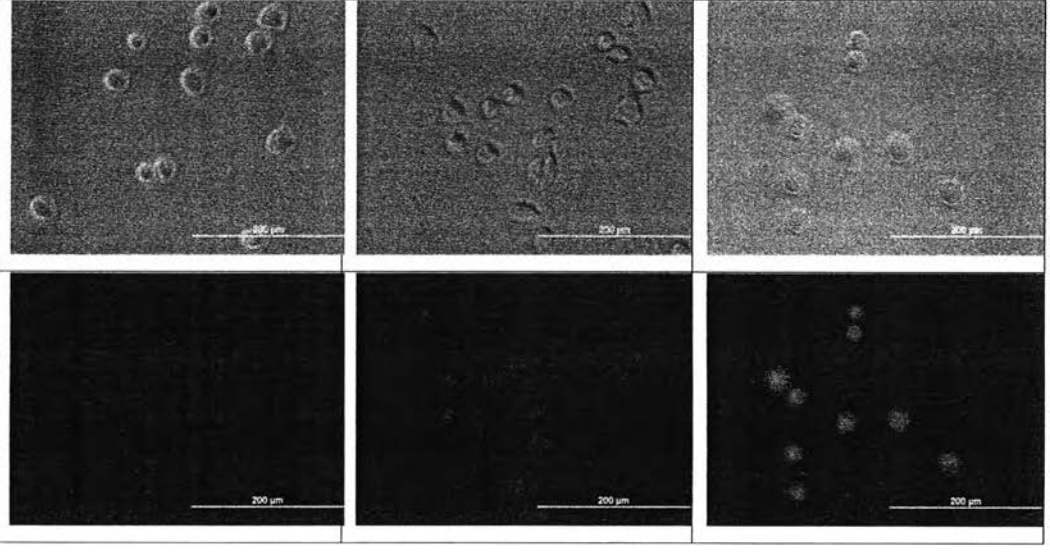 | | |

| Time | 10 μg/mL Cur in 10% DMSO/HEPES | 10 μg/mL GdSH-Cur CNPs in HEPES | 25 μg/mL GdSH-Cur CNPs in HEPES |
|---|---|---|---|
| 24 h | 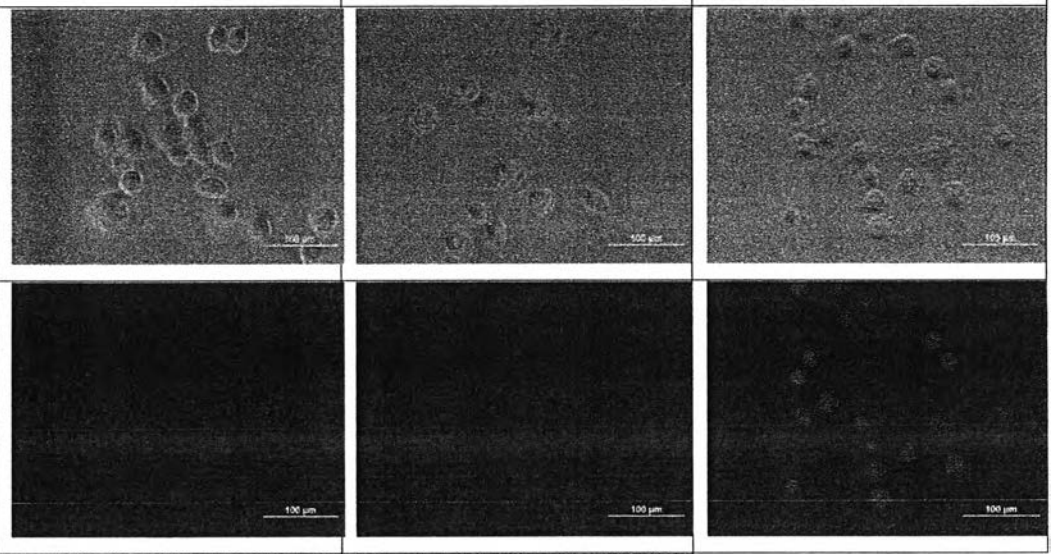 | | |
| 48 h | 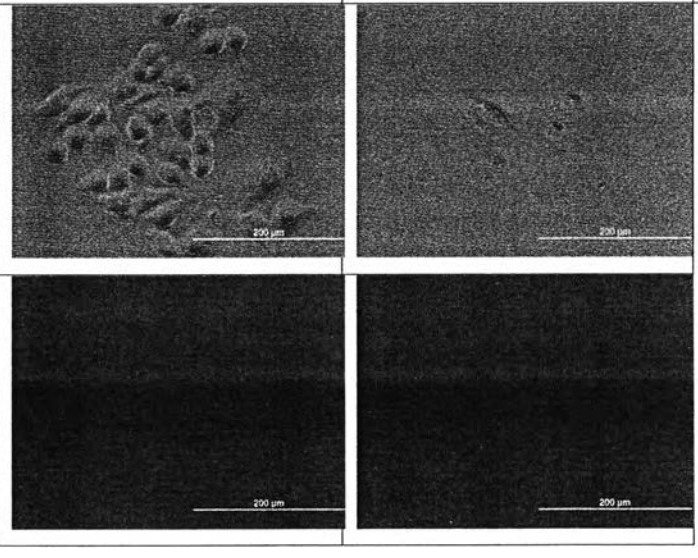 | | |

From Table 4.7, the bright field images and florescence images exhibited the comparison of SW620 cells treated with 10 μg/ml **Cur** (dissolved in 10% DMSO/HEPES) and 10 μg/ml **GdSH-Cur CNPs** (dissolved in HEPES) for 1-48 h as shown in left and middle column, respectively. The fluorescence intensity of SW620 cells incubated with **GdSH-Cur CNPs** showed more slight brightness than that incubated with **Cur**. It indicated that **Cur** in **CNPs** was possibly more stable than free **Cur** when dissolved in HEPES buffer solution. However, these samples at **curcumin** equivalent dose 10 μg/mL showed a weak fluorescence brightness of SW620 cancer cells. To intense the brightness of fluorescence image, the **GdSH-Cur CNPs** dose at 25 μg/mL was used to examine. This approach addressed the strong fluorescence

images of cells as shown in the right column of Table 4.7. The fluorescence images of SW620 cells showed an increase of fluorescence intensity as a function of the incubation time for up to 6 h. The fluorescence intensity slightly decreased after 24 h of incubation. Green fluorescence of cells, which was incubated in **GdSH-Cur CNPs** for 1 h showed immediately internalization of nanoparticles in the cells.

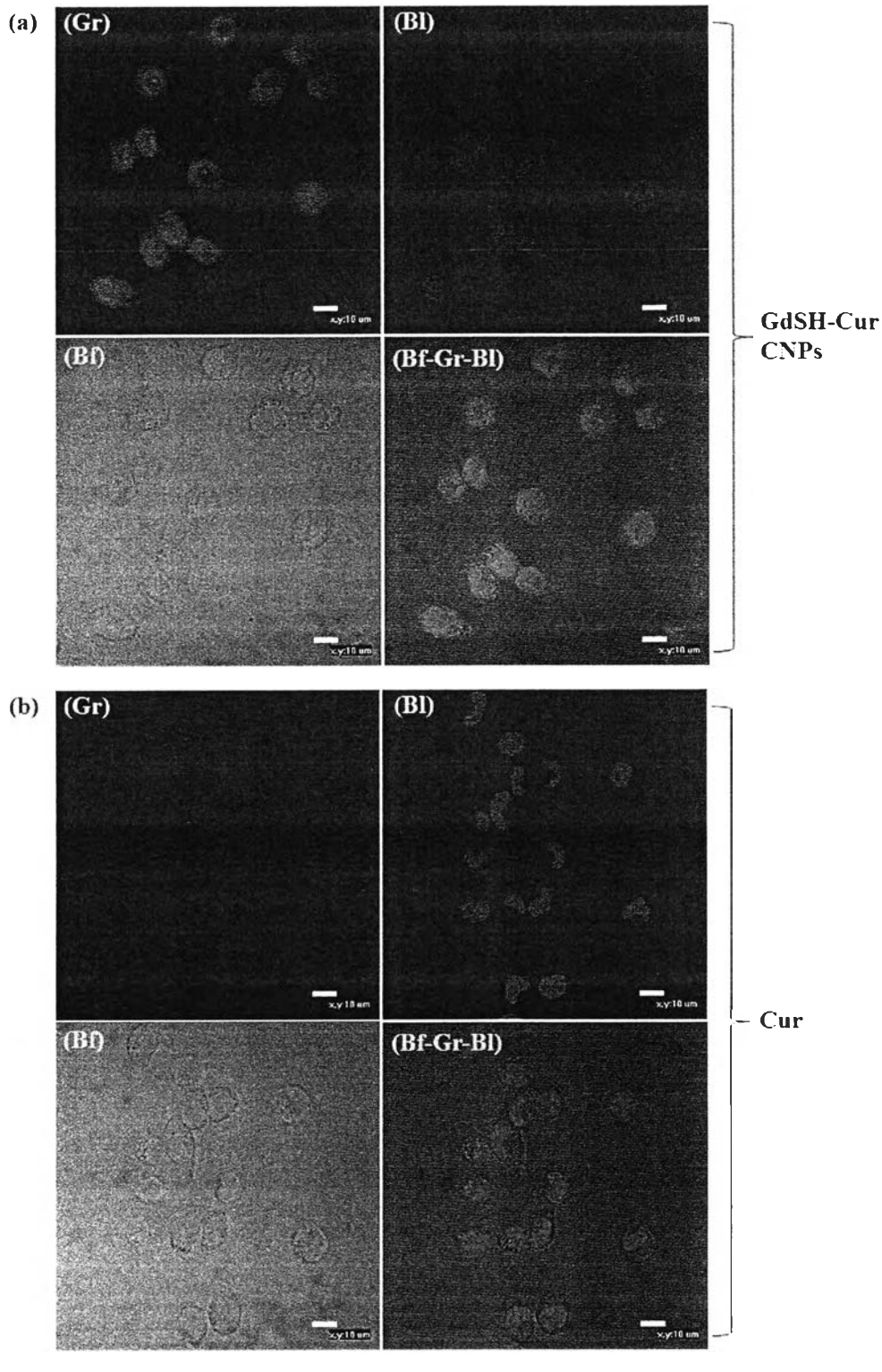

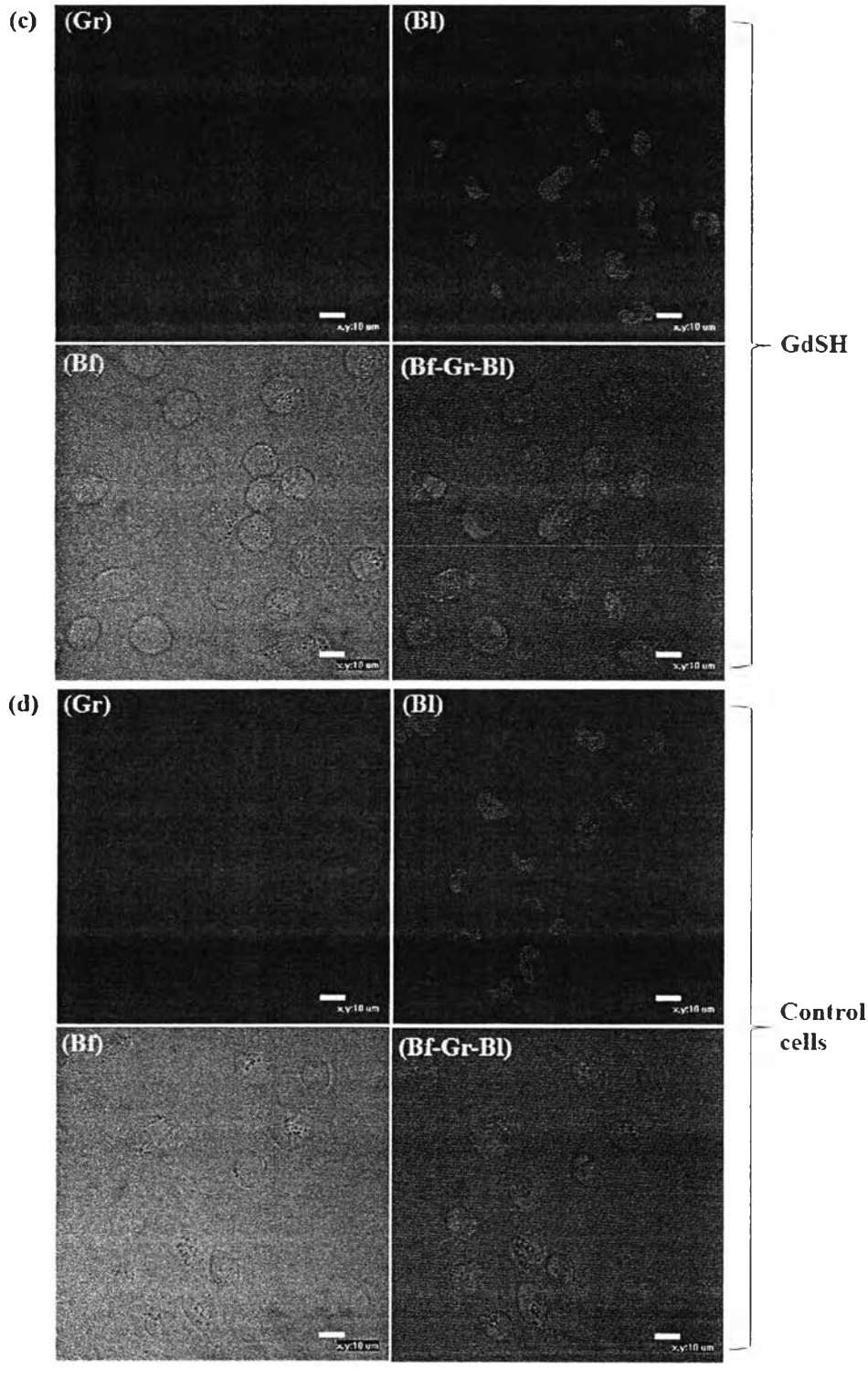


**Figure 4.41** Confocal images of SW620 cells by using confocal fluorescence microscopy were incubated in **GdSH-Cur CNPs** (a), free **Cur** (b), **GdSH CNPs** (c) and control cells (d). All of the **CNPs** and free **curcumin** were dissolved in HEPES buffer solution pH 7.4 and 10% DMSO/HEPES, respectively. The **GdSH-Cur CNPs** channel (Green; Gr), the nuclear dye channel (Blue; Bl), the brightfield image (Bf) and the merge of three channels were showed from left to right column.

To investigate the cellular uptake in SW620 cells of candidate samples, the high concentration of **curcumin** equivalent dose in range of 25 μg/mL was selected. SW620 cells were incubated with **GdSH-Cur CNPs** in 25 μg/mL of **curcumin** equivalent dose for 4 h. The comparative fluorescence images of SW620 cells incubated with **GdSH-Cur CNPs,** free **Cur**, **GdSH CNPs** and control cells without any compounds were measured by confocal laser scanning microscopy. The green channel as shown in Figure 4.41(a), confirmed that the **GdSH-Cur CNPs** were internalized into all cells. The merged image of three channels (right column) showed that the **GdSH-Cur CNPs** were localized in the cytoplasm and nucleus. In addition, the cells incubated by **GdSH-Cur CNPs** showed greater confocal fluorescence intensity than that incubated by free **Cur** (Figure 4.41(b)). The cells incubated by **GdSH CNPs** and control cells exhibited non-fluorescence (Figure 4.41(c,d)). This confirmed that **GdSH-Cur CNPs** performed a high stability in HEPES buffer solution pH 7.4. The pathway of **CNPs** passed thought the SW620 cell membrane did not clearly verify. In comparative works, the previous research has reported that **curcumin** chitosan nanocarrier was delivered into the cells and then, **curcumin** was released from NPs matrix within the cell. This performance revealed the anti-cancer effects undergone apoptosis [7]. Thereby, the fluorescence image in cell was implied that **GdSH-Cur CNPs** was rapidly internalized in the cell and showed a higher fluorescence intensity image than **Cur** without incorporated in **GdSH CNPs**.